Biol Cybern (2008) 98:145–169
DOI 10.1007/s00422-007-0200-2

ORIGINAL PAPER

Biological Cybernetics

Parametric spectral analysis of nonstationary fluctuations of excitatory synaptic currents

M. I. Glavinović · P. Gooria · F. Aristizabal · H. Taghirad

Received: 15 August 2007 / Accepted: 30 October 2007 / Published online: 8 December 2007

Abstract We assessed on Monte-Carlo simulated excitatory post-synaptic currents the ability of autoregressive (AR)-model fitting to evaluate their fluctuations. AR-model fitting consists of a linear filter describing the process that generates the fluctuations when driven with a white noise. Its fluctuations provide a filtered version of the signal and have a spectral density depending on the properties of the linear filter. When the spectra of the non-stationary fluctuations of excitatory post-synaptic currents were estimated by fitting AR-models to the segments of current fluctuations, assumed to be stationary and independent, the parameter and spectral estimates were scattered. The scatter was much reduced if the time-variant AR-models were fitted using stochastic adaptive estimators (Kalman, recursive least squares and least mean squares). The ability of time-variant AR-models to accurately fit the current fluctuations was monitored by comparing the fluctuations with predicted fluctuations, and by evaluating the model-learning rate. The median frequency of current fluctuations, which could be rapidly tracked and estimated from the individual quantal events (either Monte-Carlo simulated or recorded from pyramidal neurons of rat hippocampus), rose during the rise phase, before declining to a lower steady-state level during the decay phase of quantal event, whereas the variance showed a broad peak. The closing rate of AMPA channels directly affects the steady-state median frequency, whereas the transient peak can be modulated by a variety of factors—number of molecules released, ability of glutamate molecules to re-enter the synaptic cleft, diffusion constant of glutamate in the cleft and opening rate of AMPA channels. In each case, the effect on the amplitude and decay time of mEPSCs and on the current fluctuations differs. Each factor thus leaves its own kinetic fingerprint arguing that the contribution of such factors can be inferred from the combined kinetic properties of individual mEPSCs.

M. I. Glavinović (✉)
Department of Physiology, McGill University,
3655 Sir William Osler Promenade,
Montreal, Quebec, H3G 1Y6, Canada
e-mail: mladen.glavinovic@mcgill.ca

P. Gooria
Department of Electrical and Computer Engineering,
McGill University, Montreal, Quebec, Canada

F. Aristizabal
Department of Chemical Engineering,
McGill University, Montreal, Quebec, Canada

H. Taghirad
Center for Intelligent Machines, McGill University,
Montreal, Quebec, Canada

1 Introduction

The analysis of current fluctuations or noise analysis has been widely used in the past for the study of stochastic nature of membrane currents, and was very important in understanding the basic properties of ion conduction across membranes (Derksen and Verveen 1966; Katz and Miledi 1972; Fishman 1973). At present the method is used when the single channel conductance is low and channels inaccessible, as is often the case with synaptic currents in the central nervous system (Robinson et al. 1991; Traynelis and Jaramillo 1998; Benke et al. 2001; Mozrzymas 2004). It is now clear that the fluctuations of the excitatory post-synaptic currents are highly non-stationary (Aristizabal and Glavinović 2003). A high degree of non-stationarity is not surprising given the time course of glutamate concentration in the synapse, which rises very quickly and decays in a multi-exponential manner, though more slowly (Clements 1996; Glavinović and Rabie 1998), and the concentration dependence of several

rates of the kinetic scheme of AMPA channels (Colquhoun et al. 1992). Moreover, the desensitization of AMPA receptors, which develops rapidly during the time course of unitary excitatory post-synaptic currents, contributes significantly to shaping the time course of mEPSCs (Jones and Westbrook 1996; Glavinović and Rabie 1998; Hirasawa et al. 2001; Wall et al. 2002; Jackson et al. 2003; Yelshansky et al. 2004). The gating mechanism of transmitter-activated channels, such as ACh and AMPA channels are complex (Katz and Thesleff 1957; Trussell and Fischbach 1989), and their desensitization is associated with a progressively changing pattern of bursts and clusters (Sakmann et al. 1980), which renders the spectra of their current fluctuations non-stationary, even when activated by constant and spatially uniform pulses of transmitter (Aristizabal and Glavinović 2003). An assessment of the spectral or variance changes of non-stationary current fluctuations ought to provide important insights into the time course of the transmitter in the synaptic cleft, and the kinetics of gating of transmitter-activated channels. It would be especially valuable if it were available from individual quantal events. The highly non-stationary nature of synaptic current fluctuations requires estimates of the spectral density simultaneously in time and frequency. Traditional Fourier analysis requires much longer current segments than the mean channel open time (Silberberg and Magleby 1993). Even if the individual quantal event is taken as a single current segment its duration is rarely so long. Wavelet transform, which localizes not only in frequency but also in time, and which has a frequency dependent windowing, provides an alternative (Rioul and Vetterli 1991; Aristizabal and Glavinović 2003).

In this study, we explore how much the time-frequency resolution and accuracy can be further improved by a parametric spectral analysis (Rao 1970; Grenier 1983; Pardey et al. 1996). The parametric spectral methods differ from the non-parametric methods as they provide, not only the graphic representation of the spectral estimates (which the non-parametric methods such as Fourier and Wavelet also give), but also their representation in a compact mathematical form, i.e. they not only provide the spectral estimates but also the model parameters. Moreover, the model fits provide a filtered version of the signal, from which a significant fraction of the extraneous noise is removed. What is less clear is whether the time-invariant autoregressive (AR) models can be used to fit the segments of current fluctuations, which are assumed to be stationary and independent. If the current fluctuations are highly non-stationary the estimates of AR parameters and variables (such as the variance and the frequency of current fluctuations) are likely to be scattered (Pardey et al. 1996). We, therefore, used not only the static, but also the AR-models with the time-varying parameters for model fitting. Several 'stochastic' adaptive approaches are known: (1) the least mean square algorithm (LMS), (2) the recursive least square (RLS) algorithm and (3) Kalman filter. Static AR-model fitting provided scattered estimates of AR parameters or variables (variance and median frequency of current fluctuations), but the adaptive AR-model fitting provided smooth and accurate estimates even when the spectral or variance properties of the current fluctuations changed rapidly. Moreover, the estimates could be determined from individual quantal events.

A preliminary account has appeared (Krnjević and Glavinović 1999).

2 Methods

2.1 Solutions and recording and graphical presentation

The experiments were performed on brain slices of Sprague-Dawley (100–125 g) rats (Dingledine 1984). The rats were anaesthetized with ether and decapitated. The brain was then rapidly removed, and immersed in oxygenated (95% O_2, 5% CO_2) ice-cold artificial cerebrospinal fluid (ACSF) of the following composition (mM): NaCl 125, KCl 3, $CaCl_2$ 2, $MgCl_2$ 1.3, $NaHCO_3$ 26, NaH_2PO_4 1.25 and glucose 10, and gassed with 95% O2 and 5% CO2 (pH 7.3). Patch pipettes were filled with (mM): CsCl, 130; NaCl, 10; ATP-Mg, 3; GTP 0.3; 4-(2-hydroxyethyl)-1-piperazineethanesulphonic acid (HEPES), 10; ethyleneglycol-bis(amino-ethylether) N,N,N′,N′-tetra-acetic acid (EGTA), 10; pH was adjusted to 7.2–7.3 with NaOH. The osmolarity of the internal solution was routinely measured, and ranged from 295 to 300 $mOsm^{-1}$. Caesium was chosen as the main cation in order to block potassium conductances.

Hippocampal slices (400 μm thick) were cut using a Campden microslicer and incubated at room temperature in ACSF for at least 1 h before use. The slices were subsequently transferred to a recording chamber in which they were kept fully submerged in ACSF, flowing at 3.0–4.0 ml min^{-1}, at 27°C to which tetrodotoxin (TTX;1 mM) and bicuculline methiodide (10 μM) were added (at least 10 min before recordings started) to suppress action potential-dependent transmitter release and inhibitory ($GABA_A$) synaptic currents. Spontaneous miniature excitatory postsynaptic currents (mEPSC's) were recorded 'blindly' (Isaacson and Nicoll 1991), in the deeper areas of the pyramidal cell layer of the CA1 region using a whole cell patch clamp recording system (Axopatch-1D; Axon Instruments, Foster City CA, USA). The holding potential was −60 mV. At the end of all experiments kynurenic acid (1 mM) was added to the bath solution. A complete blockade of all synaptic activity was evidence that the spontaneous unitary events were mEPSCs. DL-2-amino-5-phosphonovaleric acid (APV - 10 μM; Sigma; Lot No 108F3810) was used to block NMDA activated channels.

The series resistance, which ranged from 3 to 8 MΩ, was not compensated to obtain low noise recordings, but was monitored throughout the experiment. If it changed by more than 15% the cell was abandoned. Data were stored on a videotape recorder (RCA) with a VCR adapter (Model PCM-4, Medical Systems). They were subsequently replayed, anti-alias filtered with a Bessel filter whose corner frequency was set at 5 kHz, and digitized with Axotape software package (Axon Instruments) at 10 kHz into a computer using a Labmaster data acquisition card (Scientific Solutions) equipped with a 12-bit A/D converter, and analyzed with Axotape (Axon Instruments). The graphics were done using Origin (Microcal Software, Northampton, MA), and the simulations using Matlab (MathWorks Inc., Natick Mass., USA) on a Dell computer.

2.2 Monte-Carlo simulations

Synaptic transmission in the excitatory synapse in the hippocampus was simulated using a Monte-Carlo method (Wahl et al. 1996; Franks et al. 2003; Ventriglia 2004). At each discrete time step: (1) every transmitter molecule had a position (x, y, z), and was flagged either as free or bound—free molecules move randomly in all three dimensions or interact with the receptors, (2) every receptor had a fixed position and was considered to be in one of the states of a given kinetic scheme—every receptor had a finite probability of changing to another state according to the same kinetic scheme. The changes of the receptor states were assumed to be Markovian (i.e. they were assumed to depend only on their present position and not on their previous history). Since the rise time of mEPSCs is of the order of ∼100 μs, we chose a 0.1 μs time step in our simulation (see below; Wahl et al. 1996).

The distance traveled by a transmitter molecule (in each of the three dimensions) was chosen randomly from a Gaussian distribution with a zero mean and a standard deviation σ given by

$$\sigma = \sqrt{2D\delta t} \tag{1}$$

(Glavinović 2002), where the δt is the length of the time step and D is the diffusion coefficient of the transmitter molecule. The random numbers were obtained from a random number generator. The diffusion in a restricted space was simulated by assuming that the transmitter molecules collide elastically with the 'walls' of the space (presynaptic or postsynaptic membranes). Finally, all molecules that reach the synaptic edge and diffuse 'away' into the 'infinite' space (similarly bound by two membranes but lacking receptors), or return from it into the synaptic cleft, were also followed. In some simulations however, glutamate molecules, which exited from the synaptic cleft were not permitted to return and were removed from the system (see Sect. 3).

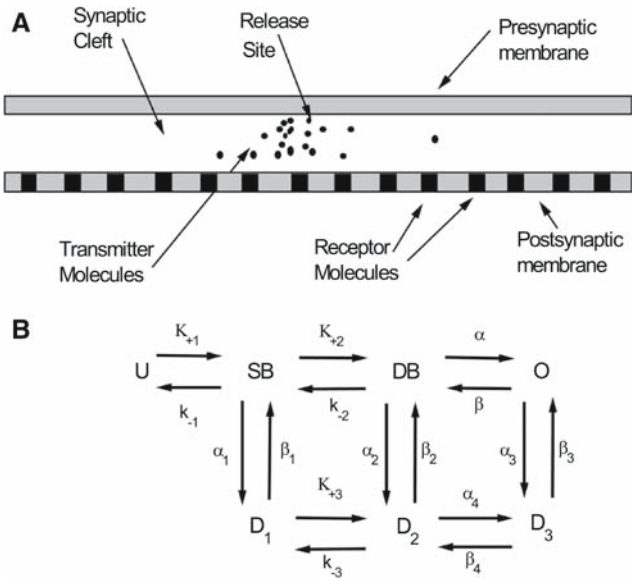

Fig. 1 Models of glutamate diffusion in the synaptic cleft and the kinetics of gating of AMPA receptors. **a** Diagram (approximately to scale) depicts how glutamate molecules, after release from an instantaneous point source, diffuse in synaptic cleft; **b** kinetic scheme of gating of AMPA receptor-channels by glutamate, used for the Monte-Carlo simulations. U, SB, DB and O indicate the unbound, singly bound, doubly bound and open state, respectively. D_1, D_2 and D_3 are three desensitized states. The rate constants, taken from Jonas et al. (1993), were adjusted for the temperature of simulations (37°C), assuming a Q_{10} of 3.0. They are: $K_{+1} = 2.38 \times 10^7 \mathrm{M}^{-1}\mathrm{s}^{-1}$, $k_{-1} = 2.22 \times 10^4 \mathrm{s}^{-1}$, $K_{+2} = 14.8 \times 10^7 \mathrm{M}^{-1}\mathrm{s}^{-1}$, $k_{-2} = 1.69 \times 10^4 \mathrm{s}^{-1}$, $K_{+3} = 6.60 \times 10^6 \mathrm{M}^{-1}\mathrm{s}^{-1}$, $k_{-3} = 237 \mathrm{s}^{-1}$ for glutamate binding; $\alpha = 2.203 \times 10^4 \mathrm{s}^{-1}$, $\beta = 4676\ \mathrm{s}^{-1}$, for channel opening; and $\alpha_1 = 1.50 \times 10^4 \mathrm{s}^{-1}$, $\beta_1 = 204 \mathrm{s}^{-1}$, $\alpha_2 = 894 \mathrm{s}^{-1}$, $\beta_2 = 3.78 \mathrm{s}^{-1}$, $\alpha_3 = 92.0 \mathrm{s}^{-1}$, $\beta_3 = 20.8 \mathrm{s}^{-1}$, $\alpha_4 = 87.3 \mathrm{s}^{-1}$, $\beta_4 = 989 \mathrm{s}^{-1}$ for the desensitization pathway. In some simulations α or alternatively β were reduced to 1/2, 1/4 or 1/8 of the above values

Synaptic transmission was simulated with glutamate released from an instantaneous point source facing the synaptic cleft, in the center of the synapse, on the membrane opposite to where the post-synaptic AMPA receptors lie (Fig. 1a). The synaptic dimensions were 200 × 200 × 15 nm; 14 × 14 (or 196) AMPA receptors were distributed equidistantly on the post-synaptic surface (Wahl et al. 1996; Glavinović and Rabie 1998). The kinetic scheme used was as given by Jonas et al. (1993, Fig. 1b). In all simulations, the temperature was assumed to be 37°C. All rates were adjusted by assuming $Q_{10} = 3.0$ and using the following equation:

$$K_{t2} = K_{t1} \times Q_{10}^{(t2-t1)/10} \tag{2}$$

where the rates at temperatures $t1$ and $t2$ are K_{t1} and K_{t2}. The diffusion coefficient of glutamine ($D = 760 \mu\mathrm{m}^2\mathrm{s}^{-1}$ measured in water at 25°C; Longsworth 1953), was the diffusion coefficient of glutamate in bulk and adjusted for the temperature difference by assuming $Q_{10} = 1.3$ (Wahl et al. 1996; Glavinović and Rabie 1998; Ventriglia 2004). Lower diffusion constants (one eighth to one half of the above value) were

also used (see Sect. 3). The single channel current amplitude was 1 pA.

According to the kinetic scheme of channel gating (Fig. 1b) a receptor can be unbound (UB), in a single or in a double bound state (SB and DB respectively; these are also called activatable states), open (O), or in one of the three desensitized states (D_1, D_2 and D_3). Each state of the receptor is associated with a surface area and a probability of binding, given that a transmitter molecule "hits" this receptor surface (Glavinović and Rabie 1998). The inverse of the receptor surface area is taken to be the density of the receptor molecules (σ_r) at the postsynaptic membrane. The probability (P_b) that a transmitter molecule, after hitting the receptor surface, will bind in a given time step (δt) is related to the macroscopic rate constant by

$$P_b = ((\sigma_r \kappa)/N_a)\left(\sqrt{(\pi \delta t)/D}\right. \tag{3}$$

where N_a is Avogadro number and κ is the appropriate rate constant of binding (in M^{-1} s^{-1}). For steps in the kinetic scheme that did not involve binding of the transmitter, the probability (p) that a receptor will move to a new state in a given time step (δt) is related to the macroscopic rate constant by

$$p = 1 - e^{-k\delta t} \tag{4}$$

where k is the appropriate rate constant (in s^{-1}). The time step (chosen to be 0.1 μs in all our calculations) was such that the probability of a receptor changing state twice within one time step was <1%. Reducing the time step further does not make the results more accurate (Wahl et al. 1996). Equation 3 also applies to the situation when a transmitter molecule unbinds from a receptor. At unbinding each molecule was moved the mean length of the random jump (0.67σ) perpendicularly away from the receptor surface: (1) to ensure that the probability of a given receptor making a transition to a bound state does not depend on the receptor's previous history; and (2) because such physical separation between the neurotransmitter and the receptor accurately reproduces the macroscopic unbinding rate constant (Wahl et al. 1996).

2.3 State–space representation of nonstationary time series

There is often a need to approximate various processes in physics, engineering and biology with mathematical models. One class of such processes is the time series. What characterizes such processes is that only the output is available whereas the input is not. Widely used models of such processes are autoregressive moving average or ARMA models. ARMA model describes the signal y_t as:

$$y_t = -\sum_{j=1}^{p} a_t^j y_{t-j} + \sum_{k=1}^{q} b_t^k e_{t-k} + e_t \tag{5}$$

where a_t^j and b_t^k are ARMA parameters at time t and e_t is the measurement error. If the processes underlying the time series are stationary, the parameters are constant.

If we denote

$$\theta_t = [-a_t^1, -a_t^2, \ldots - a_t^p, b_t^1, b_t^2, \ldots b_t^q]^T \tag{6}$$

$$\Phi_t = [y_{t-1}, y_{t-2}, \ldots y_{t-p}, e_{t-1}, e_{t-2}, e_{t-q}]^T \tag{7}$$

the time-varying ARMA model can be recast into a matrix form and be written as:

$$y_t = \Phi_t^T \theta_t + e_t. \tag{8}$$

This is a linear observation model of the time series, whereby Φ_t indicates the regression vector and θ_t indicates the model parameters. The order of the ARMA process is (p, q), where p and q are non-negative integers. The models for which a_t^j coefficients are zero are called moving average (MA) models, and those whose b_t^k coefficients are all zero are called autoregressive (AR) models. The non-stationary fluctuations of excitatory post-synaptic currents were fitted exclusively by AR-models (see Sect. 4).

2.4 Fitting static AR-models to current fluctuation segments

The AR-models are used not only for simulation but also for fitting the signals. Given a sampled signal and assuming that a process underlying the signal is linear and stationary, the parameters describing such signals can be estimated. Several approaches exist to calculate the parameters of such models: (1) forward–backward approach, whereby the sum of a least-squares criterion for a forward model and the equivalent criterion for a time-reversed model is minimized, (2) Yule–Walker approach whereby Yule–Walker equations, calculated from sample covariances, are solved, (3) Burg's lattice-based method where the lattice filter equations are solved, using the harmonic mean of squared forward and backward predictions errors, (4) least squares approach whereby the standard sum of squared forward prediction errors is minimized. The same methods may be used for non-stationary signals if parameters change very slowly. In such a case (1) the signal is segmented, (2) stationarity is assumed for each segment which are taken to be independent and (3) the parameters are determined for each segment individually.

2.5 Kalman estimation of AR-models

If their properties change rapidly, the parameter estimation of signals cannot be done adequately with non-adaptive estimation methods, as such methods assume that the parameters are stationary per window. They require adaptive methods, whereby the parameters are updated with the arrival of each data sample (Kalman 1960; Schlogl 2000; Welch and Bishop 2002; Tarvainen et al. 2004). How the 'adaptation' problem is

solved depends on the model of change of 'true' parameters. Since generally all parameters will vary in time, and in the absence of information about the nature of their change, the variation of the parameters is usually described as random walk with a white Gaussian noise, and is formally described as:

$$\theta_{t+1} = \theta_t + w_t \tag{9}$$

The goal is to find the minimum mean square estimator for state Θ_k given the observations $y_1, \ldots, y_k$. One of the most commonly used is Kalman algorithm. The equations of the Kalman estimator are:

$$\hat{\theta}_{t|t-1} = \hat{\theta}_{t-1} \tag{10}$$
$$C_{\hat{\theta}t|t-1} = C_{\hat{\theta}t-1} + C_{wt-1} \tag{11}$$
$$K_t = C_{\hat{\theta}t|t-1}\Phi_t(\Phi_t^{\mathrm{T}} C_{\hat{\theta}t|t-1}\Phi_t + C_{et})^{-1} \tag{12}$$
$$C_{\hat{\theta}t} = (I - K_t\Phi_t^{\mathrm{T}})C_{\hat{\theta}t|t-1} \tag{13}$$
$$\varepsilon_t = y_t - \Phi_k^{\mathrm{T}}\hat{\theta}_{t|t-1} \tag{14}$$
$$\hat{\theta}_t = \hat{\theta}_{t|t-1} + K_t\varepsilon_t \tag{15}$$

Given the observations $y_1, \ldots, y_{t-1}, \hat{\theta}_{t|t-1}$ is the mean square estimate of state θ_t, and $\tilde{\theta}_t = \theta_t - \hat{\theta}_t$ is the state estimation error. The unknown measurement noise e_t is replaced by the prediction error ε_t in every iteration step. Kalman gain K_{t} adjusts the state estimate following the arrival of each data sample. If we denote $P_t = C_{\theta t} + C_{wt}$ the recursive formulas become:

$$\hat{\theta}_t = \hat{\theta}_{t-1} + K_t\varepsilon_t \tag{16}$$
$$\varepsilon_t = y_t - \Phi_k^{\mathrm{T}}\hat{\theta}_{t-1} \tag{17}$$

and K_t and P_t are then transformed into:

$$K_t = P_{t-1}\Phi_t(\Phi_t^{\mathrm{T}} P_{t-1}\Phi_t + C_{et})^{-1} \tag{18}$$
$$P_t = (I - K_t\Phi_t^{\mathrm{T}})P_{t-1} + C_{wt} \tag{19}$$

Though the above equations may appear complex the meaning of Kalman adaptation can be easily understood intuitively. The goal of Kalman estimation is to compute the parameters of the AR-model at time t as a linear combination of the parameters of the AR-model at time t-1 and a weighted difference between an actual measurement at time t (in our case the current fluctuation) and its prediction at time t based on the AR-model estimated at time t-1. As the inspection of the K_t (Kalman gain) reveals, if the measurement noise (C_{et}) is small, K_t will be large, i.e. a lot of credibility will be given to the measurement, when computing the next value of y. In contrast, if the measurement noise is large, K_t will be small, i.e. very little credibility will be given to the measurement when computing the next value of y.

Table 1 Kalman gain K_t vectors K_t and covariance estimates P_t for RLS, LMS and Kalman filter (KF) algorithms

	K_t	P_t
RLS	$P_{t-1}\Phi_t(\Phi_t^{\mathrm{T}} P_{t-1}\Phi_t + \chi)^{-1}$	$\chi^{-1}(I - K_t\Phi_t^{\mathrm{T}})P_{t-1}$
LMS	$\mu\Phi_t$	$\mu(I - \mu\Phi_{t+1}\Phi_{t+1}^{\mathrm{T}})^{-1}$
KF	$P_{t-1}\Phi_t(\Phi_t^{\mathrm{T}} P_{t-1}\Phi_t + C_{et})^{-1}$	$(I - K_t\Phi_t^{\mathrm{T}})P_{t-1} + C_{wt}$

Note however, that in addition to the Kalman algorithm several other adaptive algorithms are now available (Haykin 1986; Sayed and Kailath 1994; Schlogl 2000). Table 1 shows how K_t and P_t were defined in this study for Kalman, RLS and LMS estimators. Whereas the gain K_t controls the adaptation of the Kalman estimator, χ—the forgetting factor, and μ—the step size, control the adaptation for the RLS and LMS estimators respectively. Note that the measurement and state noises e_t and w_t are assumed to be uncorrelated, Gausssian white noise processes with zero mean and with covariances $C_{et} = \sigma_e^2$ and $C_{wt} = \sigma_w^2 I$, respectively. Process noise reflects the error propagation in the model of the signal.

2.6 Spectral estimation

In case of a general ARMA (p, q) model, given the knowledge of its time-varying a_t^j and b_t^k coefficients, the time-varying power spectrum density (PSD) estimate is calculated as:

$$\mathrm{PSD}(f) = \frac{\sigma_\varepsilon^2(t)}{f_s} \frac{\left|1 + \sum_{k=1}^{q} b_t^k \mathrm{e}_{\mathrm{s}}^{-i2\pi kf/f}\right|^2}{\left|1 + \sum_{j=1}^{p} a_t^i \mathrm{e}_{\mathrm{s}}^{-i2\pi jf/f}\right|^2} \tag{20}$$

where $\sigma_\varepsilon^2(t)$ is the time-varying prediction error variance (which is used instead of the variance of the unknown white noise process) and which is calculated at every step of iteration over a window of samples; 38). f_s is the sampling frequency (Tarvainen et al. 2004). This is reduced to:

$$\mathrm{PSD}(f) = \frac{\sigma_\varepsilon^2(t)}{f_{\mathrm{s}}} \frac{1}{\left|1 + \sum_{j=1}^{p} a_t^i \mathrm{e}_{\mathrm{s}}^{-i2\pi jf/f}\right|^2} \tag{21}$$

in the case of the AR-model used in this study.

2.7 Initialization and mean learning rate

Before estimation starts, AR parameters, state noise covariance and prediction error variance must be initialized. This was done either by randomly initializing the AR parameters, zero initializing the state θ_{t0} and setting the $C_{\hat{\theta}t0}$ error

covariance to $10 \times \mathrm{I}$, where I is an identity matrix (this is termed 'random initialization') or by initializing with the values determined by passing a static AR-model over a short segment of 50–100 samples from the initial portion of the signal ('static' initialization).

It is often desirable to know how fast the filter converges to the stationary solutions, when estimating stationary signals, but also how fast it adapts to new conditions when estimating non-stationary signals. The learning rate of the Kalman filter provides such an index (DeFreitas et al. 1998). The learning rate matrix of the Kalman filter was calculated as:

$$\rho = S_i / \sigma_i, \tag{22}$$

where S_i is the uncertainty of the AR parameters whereas σ_i is the variance of the predicted signal. The learning rate is a matrix because each AR parameter adapts at a different rate to the given signal. We calculated the mean learning rate by averaging the learning rate over all AR parameters, which is equal to

$$\rho_{\mathrm{mean}} = \mathrm{Tr}(S_i)/(p \times \sigma_i) \tag{23}$$

where Tr denotes the trace of the covariance matrix and p is the number of AR parameters.

3 Results

3.1 Non-adaptive AR spectral estimation of the fluctuations of Monte-Carlo simulated spontaneous excitatory post-synaptic currents

Figure 2a depicts a miniature excitatory post-synaptic current (an mEPSC) simulated using Monte-Carlo technique (see Sect. 2), together with the best fit of two exponentials calculated using the least squares fitting method. The best-fitted equation was: $i = 157.9 \times \exp^{-t/0.468} \times (1 - \exp^{-t/0.074})$, where i is the current in pA and t is the time from the start in ms. The mEPSC fluctuations (Gaussian random noise with a zero mean and a standard deviation of 0.2 pA was added to the Monte-Carlo simulated mEPSC) are shown in Fig. 2b. The predicted fluctuations estimated using a second order AR-model are not very 'noisy' (i.e. the fluctuations are mainly due to the opening and closing of AMPA channels; Fig. 2c). This demonstrates that (assuming that the extraneous noise shows no correlation) AR-model fitting, even when non-adaptive, is highly successful in predicting the 'true' signal and filtering the extraneous noise. The innovations (defined as the difference between the AR-model prediction and the mEPSC fluctuations) are shown in Fig. 2d. However, the variance of the fluctuations predicted by AR-model fitting, and even more so the median frequency (Fig. 2e, f, respectively), are scattered, especially during the late decay phase of the mEPSC. Finally, AR parameter estimates are also highly scattered (Fig. 2g).

3.2 Kalman-AR estimation of two concatenated stationary signals with identical spectral properties but different variances

Significant improvements in estimation are possible if the adaptive, instead of non-adaptive, approaches are used. Figure 3a shows a random signal generated by a concatenation of two signals. In both cases, a zero-mean white Gaussian random signal with a unitary standard deviation was filtered by a third order Butterworth filter whose corner frequency was 0.4 kHz and sampling frequency 1 kHz. The amplitude of the first half of the signal was then multiplied by 4, and of the second half by 2. The final 'true' variances of so concatenated signals were 96.6 and 26.1, respectively. In addition a zero-mean white Gaussian random signal with a standard deviation of 0.25 was added to both segments. The Kalman-AR method (see Sect. 2) was used to: (1) estimate the parameters of the second order AR-model, (2) predict a signal based on such a model and (3) calculate the median frequency and the variance of the predicted signal. The state noise variance σ_{w}^2 was 5×10^{-4} (Tarvainen et al. 2004), whereas the window used for averaging the measurement error variance had 50 samples (Penny and Roberts 1999).

Both σ_{w}^2 and window length influenced the scatter (but not the magnitude) of the variance of the predicted signal, and the lag between the predicted and the original signal (see Sect. 2). Reducing the σ_{w}^2 lowered the scatter (compare Fig. 3c, e). This is as expected, because σ_{w}^2 controls how much model parameters are allowed to change for each new data sample. The scatter was further reduced as the window length increased. This is also not surprising because the variance of any set of data diminishes as the number of data points used for the estimation rises. In both cases, lower scatter was associated with a longer lag between the variance of the original signal (i.e. the 'true' value of the variance) and its estimate, but the lag was very small. In general thus there is a trade-off between the scatter of the estimates and the lag between the original and estimated variables. Figure 3d, f, h show how the median frequencies of the spectra of the predicted signal estimated using Kalman-AR-modeling are affected as σ_{w}^2 and window length change. The scatter of the median frequency estimates depends on σ_{w}^2 and window length in a manner very similar to that of the prediction variance (i.e. lower σ_{w}^2 and longer window lead to lower scatter). The magnitude of the median frequency remains however, independent of σ_{w}^2 or the window length. Finally, even a large and abrupt change of the signal amplitude in the middle (i.e. 3 ms from the start), had no effect on the magnitude or scatter of the median frequency estimates.

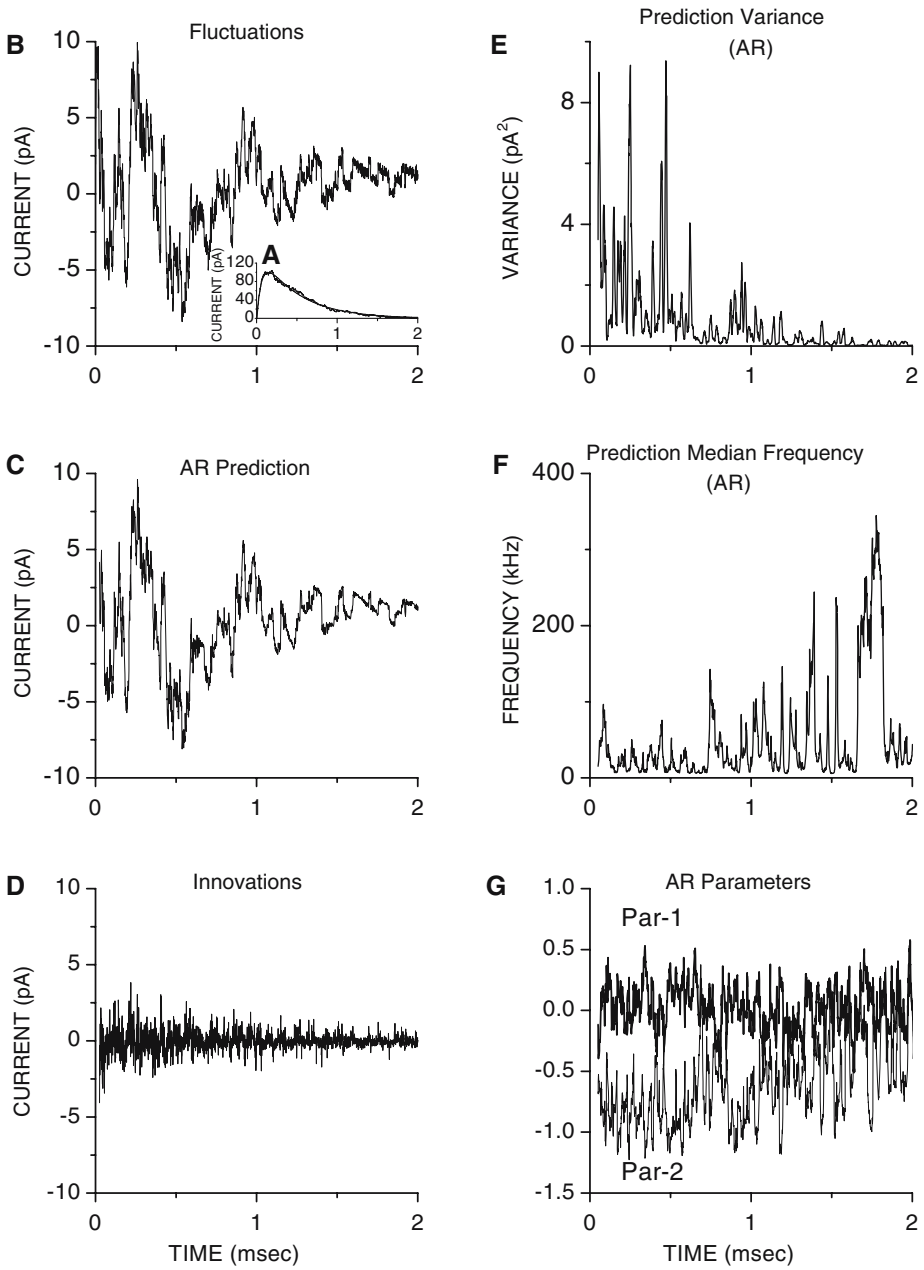

Fig. 2 Non-adaptive model fitting provides scattered estimates of AR parameters, and of variance and median frequency of current fluctuations. **a** Simulated mEPSC together with the best fit made by the sum of two exponentials. Note that a Gaussian random noise with a zero mean and a standard deviation of 0.2 pA was added to the simulated mEPSC. The amplitude of the single channel currents was 1.0 pA; **b** mEPSC fluctuations; **c** AR prediction; **d** innovations (defined as the difference between the Kalman-AR-model prediction and the signal). **e** variance of AR-prediction; **f** median frequency of AR prediction is very scattered especially during the late decay phase of mEPSC; **g** AR parameter estimates are quite scattered. Each value was predicted based on a segment of 50 data samples (the overlap of segments was maximal—49 samples)

3.3 Kalman-AR estimation of non-stationary signal generated by concatenation of time-varying AR parameters

The ability of Kalman-AR method to track the signal whose spectral properties changed rapidly was also estimated. The signal shown in Fig. 4a was generated by passing a zero-mean white Gaussian noise with a variance of 1.0 through a second order AR-model, whose first and second parameters were as shown in Figs. 4b, d (thick line). The first parameter was a concatenation of two sinusoids, which had the same bias of 0.2, and which were of equal duration and amplitude (equal to 0.5), but whose frequencies differed being 1.25 and 0.625 kHz, respectively. The second parameter was also formed by a concatenation of two sinusoids of identical amplitude of 0.2 and bias of 0.3, but unequal duration (the second part was twice as long as the first) and frequency. The frequency of the first sinusoid was 0.625 kHz and the second 1.25 kHz. Second order AR-model was used for Kalman-AR estimation. The state noise variance σ_w^2 was 5×10^{-4}, whereas the window used for averaging the variance of the prediction error σ_ε^2 had 50 samples. Note that the Kalman-AR estimation of both parameters is excellent even at the points of concatenation (Fig. 4b, d). Figure 4c shows the prediction variance

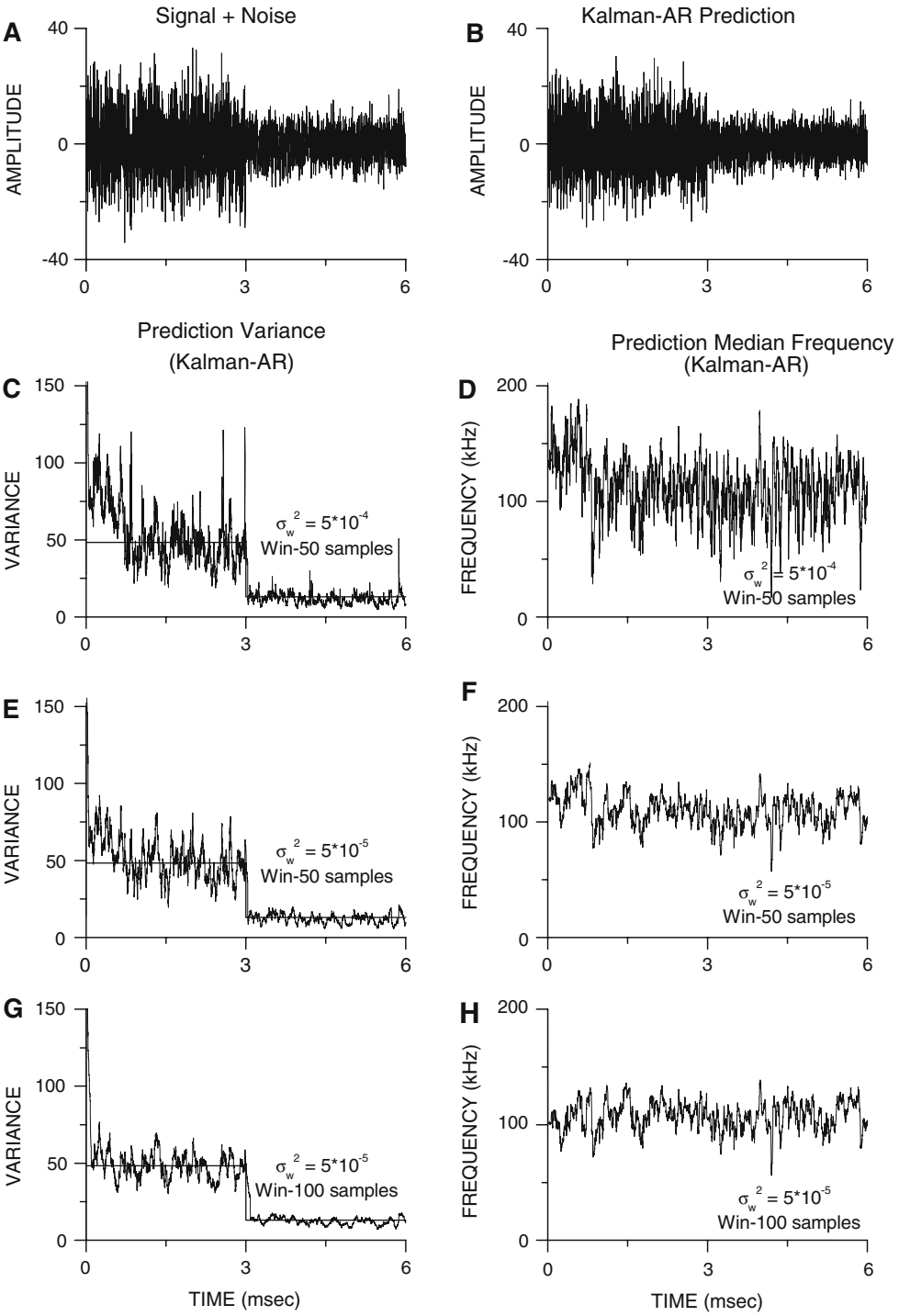

Fig. 3 Both the state noise variance σ_w^2 and the length of the averaging window affect the tracking ability of the Kalman-AR-model fitting. **a** Direct concatenation of two signals of the same duration, both generated by passing a zero-mean white Gaussian random signal with a unitary standard deviation through the same Butterworth filter (see text), subsequently multiplied by 4 and 2. Finally, a zero-mean white Gaussian random noise with a standard deviation of 0.25 was added to both signals. **b** Kalman-AR prediction estimated assuming a second order AR-model and state noise variance σ_w^2 of 5×10^{-4}; the window for averaging the prediction error variance had 50 samples. Variance (c, e and g) and median frequency (d, f and h) of the Kalman-AR prediction. The state noise variances $\sigma_w^2 s$ and averaging windows as indicated

and Fig. 4e the prediction variance. Note that the prediction error variance was clearly very close to the variance of the white noise process, which is generally unknown (its 'true' value was 1.0 and constant throughout). Finally note that the changes of the median frequency of the signal and those of the first AR parameter are similar, indicating that the first AR parameter largely determines the spectral properties of the signal.

3.4 Kalman-AR spectral estimation of the fluctuations of Monte-Carlo simulated spontaneous excitatory post-synaptic currents

Figure 5a, b depict a simulated miniature excitatory post-synaptic current (an mEPSC) with the best fit of two exponentials calculated using the least squares fitting method, and the current fluctuations to which a Gaussian random noise

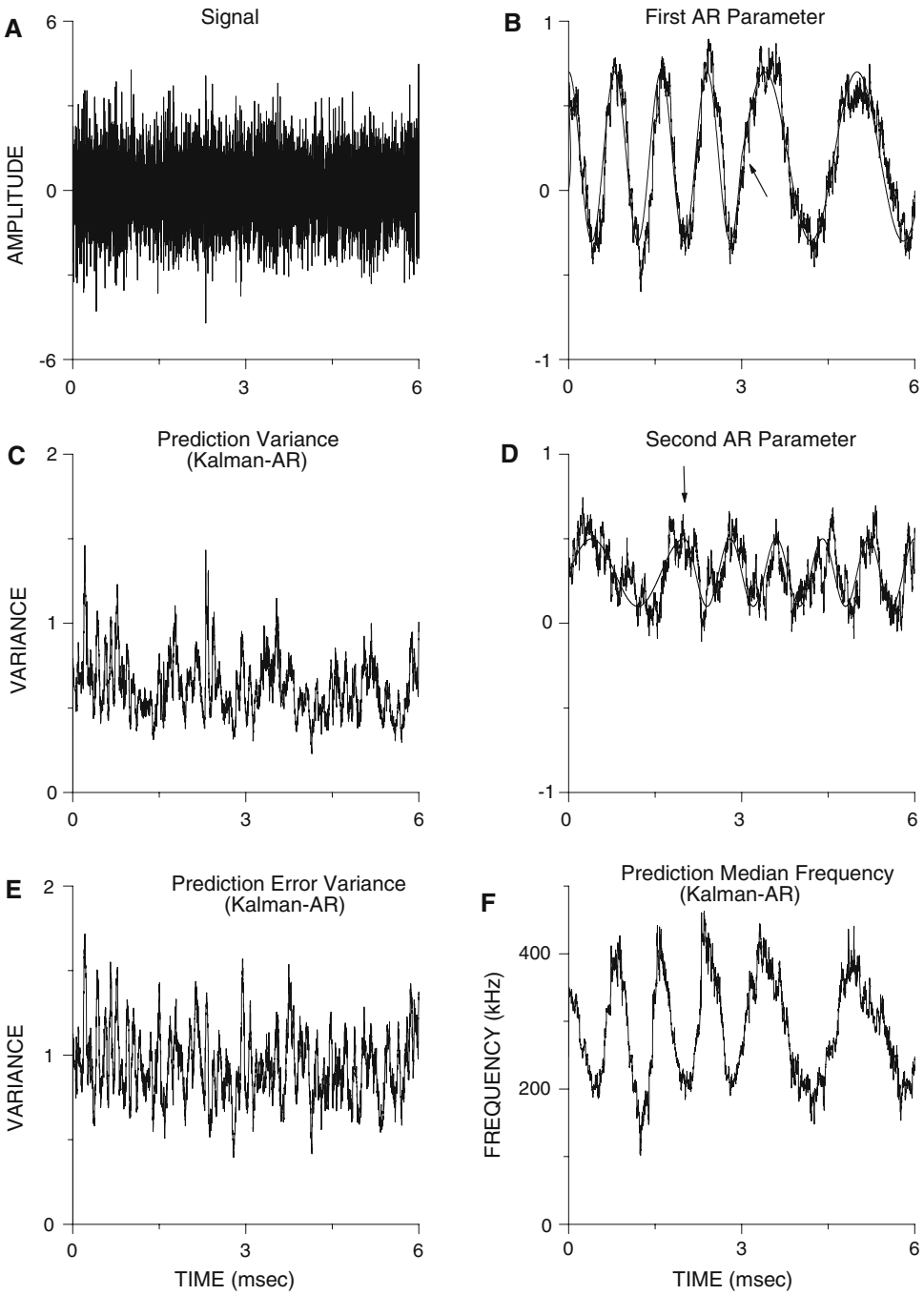

Fig. 4 Concatenation of AR parameters. **a** The signal generated by passing a zero-mean white Gaussian noise with a variance of 1.0 through a second order AR-model; **b** and **d** first and second AR parameter, respectively, were generated by a concatenation of two sinusoids (*thick lines*; see text). *Arrows* indicate the times when concatenation occurred. Kalman-AR estimates of AR parameters, (*thin lines*); **c** The prediction error variance; **e** The variance of the predicted signal; **f** median frequency of the predicted signal; Second order AR-model was used for Kalman-AR estimation, the state noise variance σ_w^2 was 5×10^{-4}, whereas the window for averaging the prediction error variance σ_ε^2 had 50 samples

with a zero mean and a standard deviation of 0.2 pA was added. Same data are shown as in Fig. 2 for a better comparison of the ability of adaptive vs. non-adaptive methods to fit the current fluctuations. Kalman-AR-model prediction of the mEPSC fluctuations is given in Fig. 5C. The AR-model used for the Kalman-AR estimation was second order, the state noise variance $\sigma_w^2 5 \times 10^{-4}$ and the window of 50 samples was used for averaging the prediction error variance σ_ε^2 (see Sect.2). The innovations (Fig. 5d) diminished with time, as did the Kalman-AR prediction error variance (or variance of innovations), which reached low but non-zero values (Fig. 5e). Finally, AR-model parameters estimated by the Kalman-AR-model fitting are shown in Fig. 5f. Following an initially moderately high level of parameter uncertainty and relatively rapid change both parameters became more stationary and very smooth as the time progressed.

The power spectra are smooth, but change with time. Near the peak of mEPSC (i.e. at 0.2 ms from the start), high frequencies of current fluctuations are more prominent than during the decay phase (i.e. at 1.0 ms from the start; Fig. 6a).

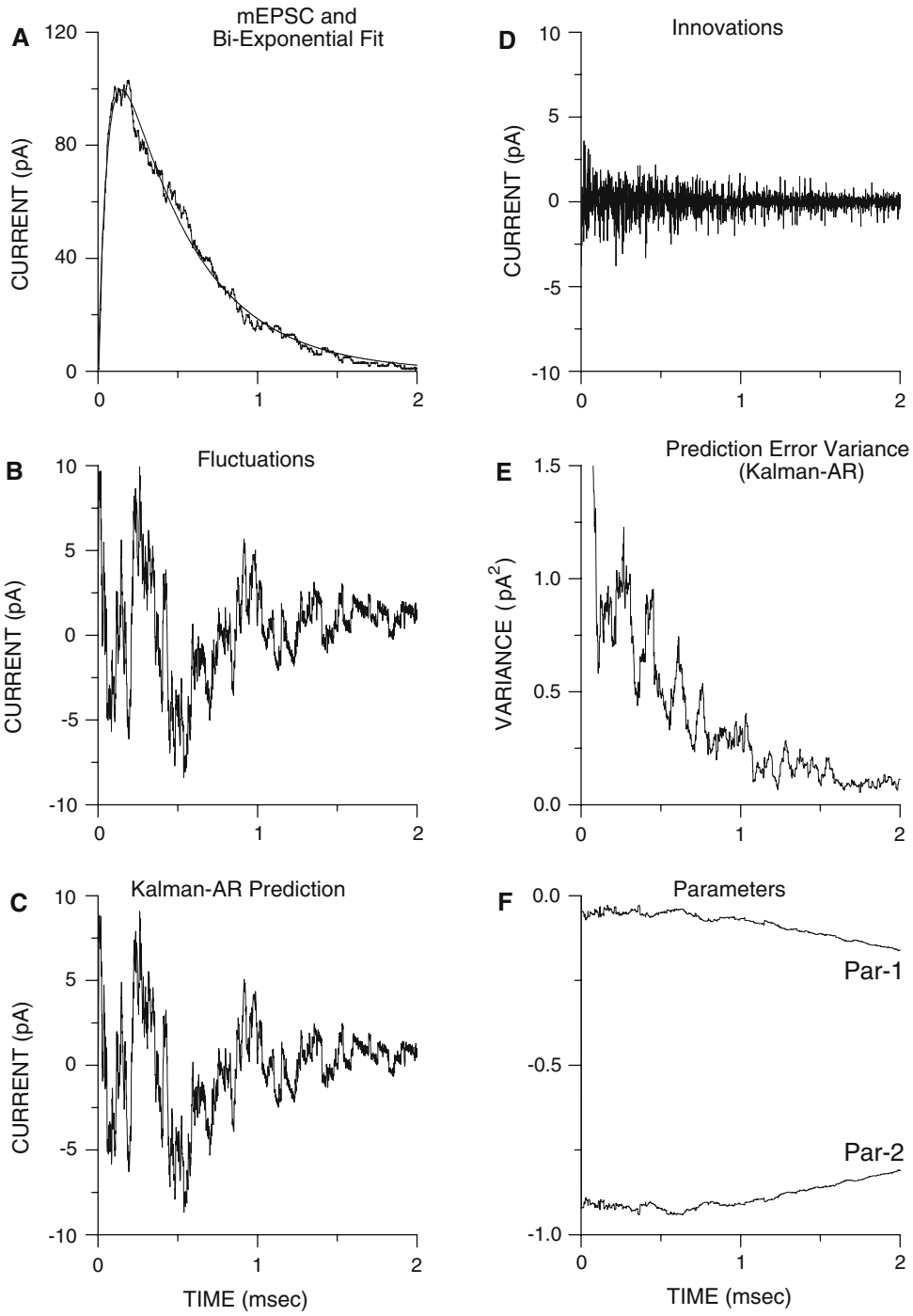

Fig. 5 Adaptive model fitting provides smooth estimates of AR parameters. **a** Simulated mEPSC with the best fit by the sum of two exponentials; **b** mEPSC fluctuations. Note that a Gaussian random noise with a zero mean and a standard deviation of 0.2 pA was added to the simulated mEPSC. The amplitude of the single channel currents was 1.0 pA. **c** Kalman-AR-model prediction of the signal. **d** the innovations. **e** the variance of the Kalman-AR prediction error. **f** AR parameters estimated by the Kalman-AR-model fitting. Note that except initially the time course of both parameters is smooth

The spectral densities do not depend on the choice of the order of the model used for Kalman-AR fitting. At 1.0 ms from the start the spectra estimated assuming a second or a fourth order were completely overlapping, and at 0.2 ms they were different at low frequencies but only marginally. The variance of the signal predicted by Kalman-AR-modeling is given in Fig. 6b. Figure 6d depicts two estimates of the median frequency. In one case, the initialization was 'random' (thin line; see Sect. 2), and in another case a short (100 samples) segment was passed through a static second order AR-model, and the values of the parameters and states thus estimated were used for initialization in Kalman-AR-model fitting ('static' initialization; see Sect. 2). The two estimates differ significantly only in the brief interval at the start but not subsequently. Higher median frequency, which is observed at the beginning, with 'random' initialization of the parameters (and zero initialization of the states) suggests that the model was unable to adapt rapidly enough to find

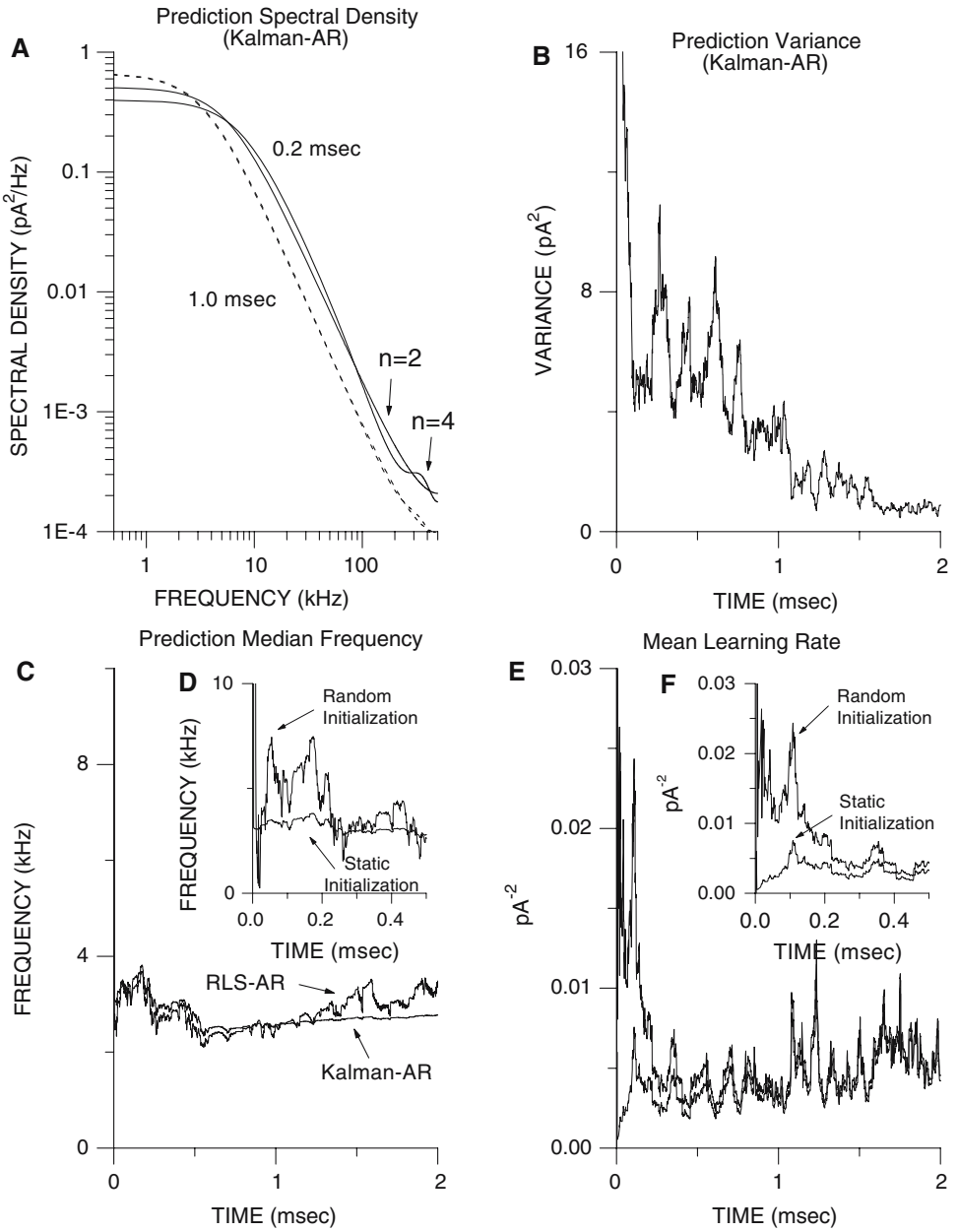

Fig. 6 Adaptive model fitting provides smooth estimates of the spectral density, but also of the variance and median frequency of mEPSC current fluctuations. **a** The power spectra of the fluctuations of Monte-Carlo simulated miniature excitatory post-synaptic current (mEPSC) 0.2 (*thick solid line*) and 1.0 ms (*thin dashed line*) from the start. *n* gives the order of the AR-model used for fitting. Some differences are visible between the spectra estimated using second order and fourth order AR-model when the estimates were made 0.2 ms from the start, and even then only for low frequencies. The spectra estimated at 1.0 ms from the start are completely overlapping. Note that the spectra are smooth although the Gaussian random noise with a zero mean and a standard deviation of 0.2 pA was added to the simulated mEPSC. The amplitude of the single channel currents was 1.0 pA; **b** variance of the Kalman-AR prediction; **c** median frequency estimates made using the Kalman-AR (*thick line*) or RLS-AR (*thin line*) are similar and change rapidly with time. The state noise variance σ_w^2 controlling Kalman adaptation was 5×10^{-9}, whereas the forgetting factor λ of RLS was 0.995 and the window for averaging the prediction error variance σ_ε^2 had 50 samples. 'Static' initialization was used in both cases; **d** median frequency of the Kalman-AR prediction using either the 'random' initialization (*thin line*) or the 'static' initialization (*thick line*);**e, f** mean learning rate of the Kalman-AR-model, though initially high, declines quickly to low levels. The mean learning rate during the rise phase of the mEPSC is lower, if the 'static' initialization instead of 'random' initialization is used

the 'true' values, partly due to the fact that the difference between the initial values of the AR parameters and states and 'true' values is large, and partly due to the fact that at the beginning AR parameters change very rapidly. Figure 6c compares the estimates of the median frequency made using RLS-AR and Kalman-AR-model fitting. In both cases the

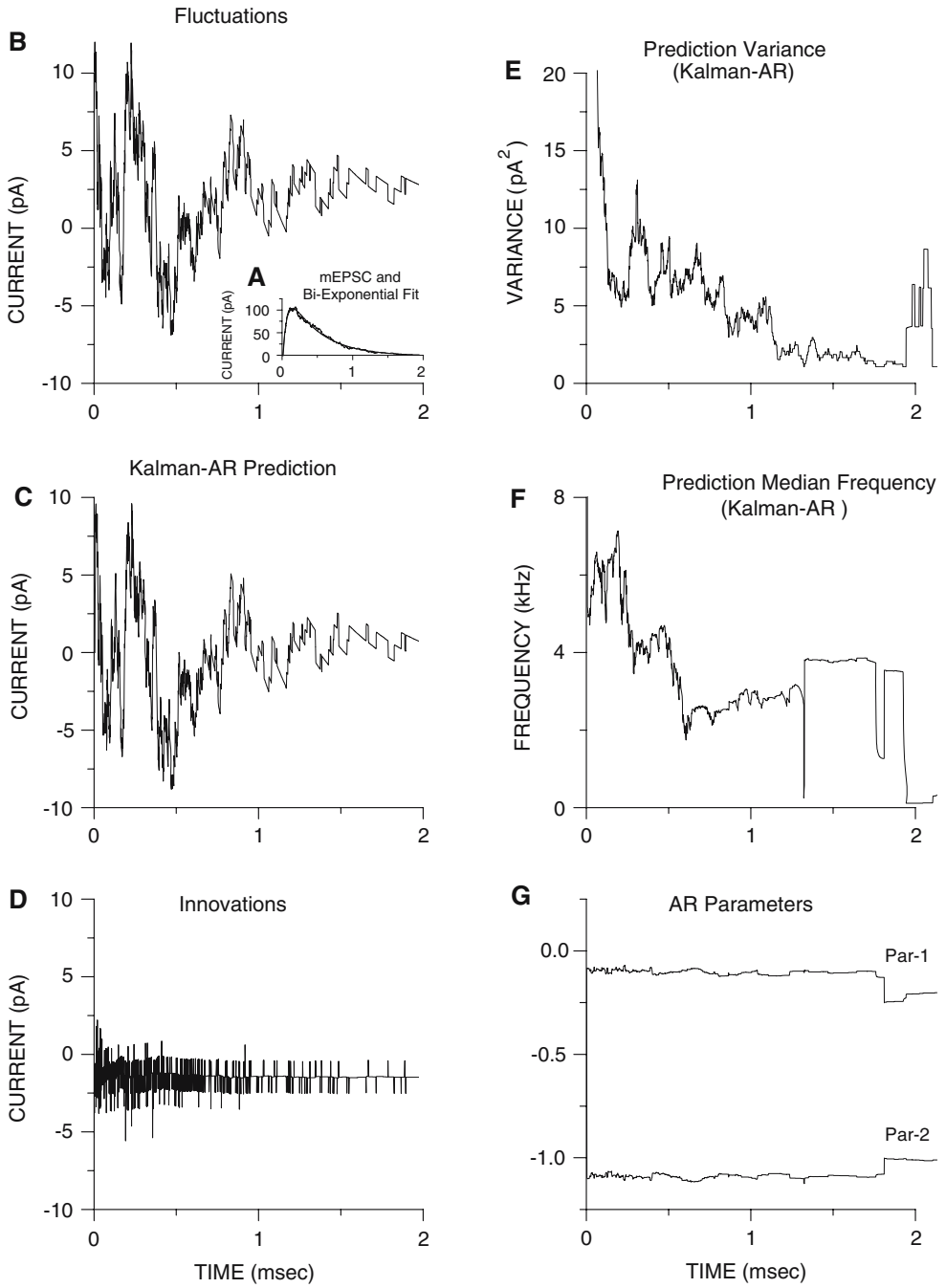

Fig. 7 Adaptive model fitting of the noiseless fluctuations of the Monte-Carlo simulated spontaneous excitatory post-synaptic currents (mEPSCs) can provide more scattered estimates of AR parameters and variance and median frequency of current fluctuations. **a** Simulated mEPSC with the best fit by the sum of two exponentials; **b** mEPSC fluctuations. Note that the fluctuations consist only of the simulated mEPSC, i.e. there is no noise added. The amplitude of the single channel currents was 1.0 pA. **c** Kalman-AR-model prediction of the signal; **d** the innovations (defined as the difference between the Kalman-AR-model prediction and the signal); **e** the Kalman-AR prediction error variance; **f** AR parameters estimated by the Kalman-AR-model fitting. Note that except initially the time course of both parameters is smooth

initialization was 'static'. The difference between two estimates is evident only at the beginning and largely disappears afterwards.

As dynamic conditions change the Kalman-AR-model adapts to the new data. The adaptation can be monitored using the mean learning rate (Penny and Roberts 1999; see Sect. 2). When the model is exposed to new data the mean learning rate is very high initially, but decreases as the model becomes exposed to the data whose properties are more stationary, i.e. well characterized by the model whose AR parameters are

more stationary and less scattered (Fig. 6e, f). The ability of the model to adapt to the new dynamical regimes and the importance of initialization in spectral tracking can be better appreciated by comparing the mean learning rate with 'random' initialization and 'static' initialization (calculated by fitting the static AR-model fitted to the short (0.1 ms) segment of data). There is a clear difference, which is more evident when shown on the expanded scale (Fig. 6f). Nevertheless, irrespective of whether the 'random' or 'static' initializations were used, after a brief interval of ∼0.1 ms the mean learning rates were essentially the same. Lower mean learning rate observed with 'static' initialization is in keeping with the idea that the parameter, state and $C_{\hat{\theta}t0}$ error covariance values obtained from the static AR-model fitted to a 100 samples data segment are closer to 'true' values than random AR parameters, zero state values and $10\times$ I (I is identity matrix) $C_{\hat{\theta}t0}$ error covariance.

Kalman-AR-model fitting of the 'noiseless' mEPSC fluctuations does not lead to highly accurate parameter, median frequency or variance estimates. Figure 7a,b depict a simulated miniature excitatory post-synaptic current (an mEPSC) with the best fit of two exponentials calculated using the least squares fitting method, and the current fluctuations (same data as in Fig. 5, but without Gaussian random noise added to the fluctuations produced by the opening and closing of the AMPA activated channels). Kalman-AR-model prediction of the mEPSC fluctuations (Fig. 7c) was estimated using the second order AR-model. The state noise variance σ_w^2 was 5×10^{-9}, and the window for averaging the prediction error variance σ_ε^2 had 50 samples (see Sect. 2). The innovations diminished with time (Fig. 7d). Figure 7e, f give the variance and the median frequency of the Kalman-AR prediction. Finally AR-model parameters estimated by the Kalman-AR-model fitting are shown in Fig. 7g. Note that the variance and the median frequency of the Kalman-AR predicted current fluctuations, as well as the estimated AR parameters are highly scattered especially during the late decay phase of the mEPSC.

3.5 Transient median frequency of current fluctuations depends not only on number of glutamate molecules released but also on their ability to re-enter into the synaptic cleft

As expected mEPSC amplitudes rise when more glutamate molecules are released, whereas the decay time remains essentially the same (Fig 8a–c). The median frequency of current fluctuations, higher during the rise phase and early decay phase, decreases to a steady level during the late decay phase. The transient median frequency depends, whereas the steady-state level is largely independent on how many molecules are released (Fig. 8f). Note that the transient median frequency is the highest when the number of glutamate molecules released is the lowest (1,500 molecules), but if 6,000 molecules are released the transient median frequency is typically higher than when 3,000 molecules are released. This dependence is puzzling. If more molecules are released the occupancy of the double bound state should rise (and it does; Fig. 8g), and this should produce higher transient median frequency. So why is the transient median frequency versus number of molecules released relationship not monotonic? The answer lies in the fact that there is an opposing tendency. The variability of the occupancy of the double bound state also influences the median frequency of the current fluctuations, and it diminishes when more molecules are released (Fig. 8h). Both the overall occupancy of the double bound state and its variability, are influenced by the similar changes of the cleft glutamate concentration and its variability (Fig. 8e), which is as expected because the rate leading into the double-bound state (from a single bound state) is concentration dependent. In all figures, the median frequency of current fluctuations and the occupancy of the double bound state are averages from six simulations. The coefficient of variation (CV=standard deviation/mean) is taken as an index of the variability. CV values of the occupancy of double bound state, or cleft glutamate concentration (which are estimated as running values of 50 individual estimates), which are shown, are also averages from six simulations.

Similar mEPSC amplitude vs. number of molecules released relationship is observed if molecules exiting from the cleft are not able to return. Although the amplitudes are significantly smaller, the decay times (which are only marginally shorter) are similarly independent of the number of molecules released (Fig 9a–c). Contrary to what is observed in the simulations where molecules are able to return to the cleft, the peak of the transient median frequency is (1) typically much greater, and (2) positively correlated with the number of molecules released (Fig. 9e). This is not surprising because both the overall occupancy of the double bound state and its variability are higher when more molecules are released (Fig. 9f,g). Finally note that these changes are not due to the changes of the glutamate concentration in the cleft, because the glutamate concentration diminishes to zero in 20–30 μs (Fig. 9d).

3.6 Slower diffusion of glutamate renders mEPSCs amplitudes greater and decay times longer but markedly reduces transient median frequency of current fluctuations

The amplitudes of mEPSCs rise, the decay times lengthen (Fig. 10a–c), whereas the peak of the transient median frequency diminishes and very significantly (Fig. 10f) when the diffusion constant of glutamate decreases from the value equal to that in the bulk solution (1,040 $\mu m^2/s$) to one-eighth

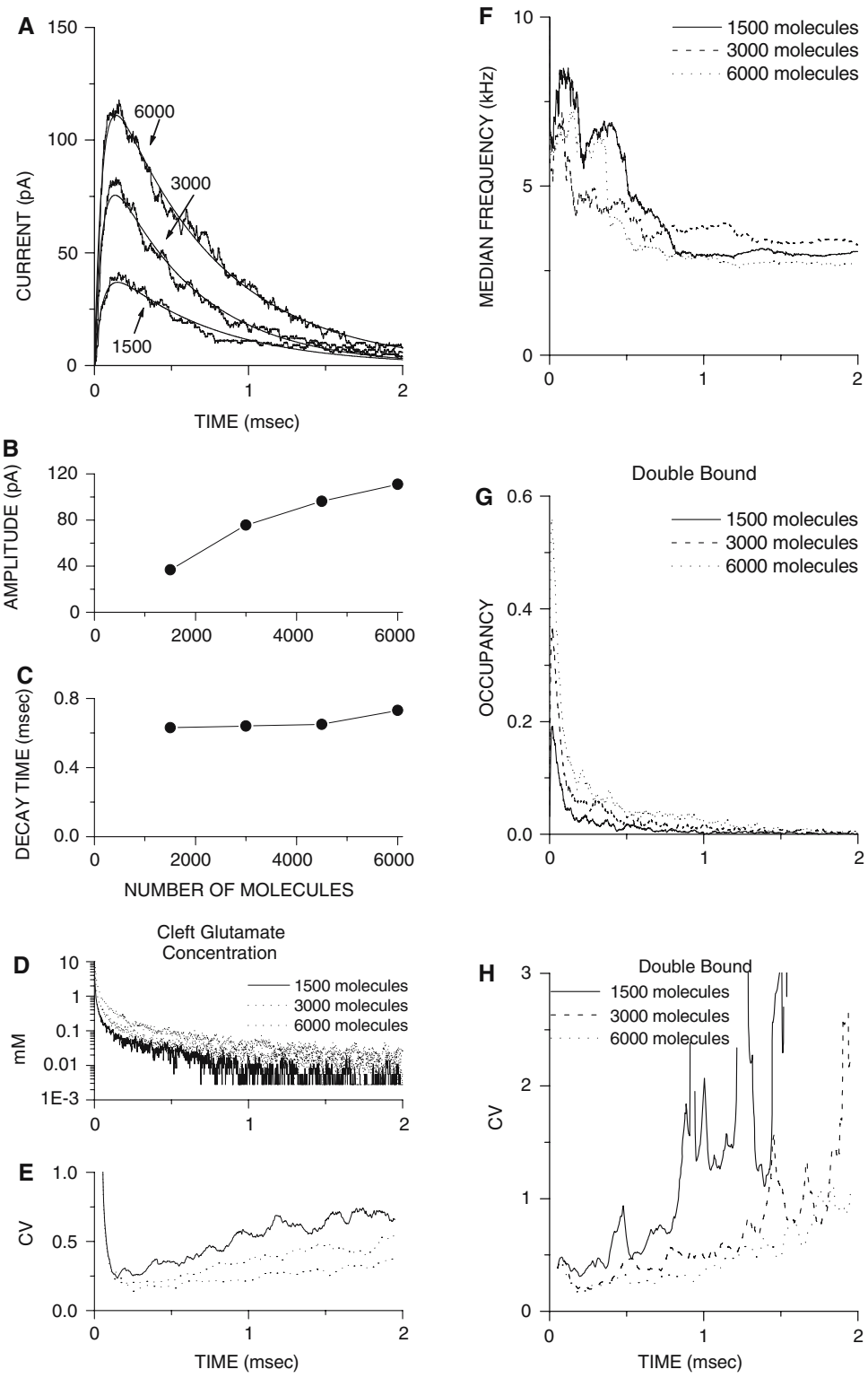

Fig. 8 Transient median frequency of the current fluctuations diminishes albeit modestly, if the number of glutamate molecules released rises, and if the glutamate molecules are able to return into the synaptic cleft (see text; **f**). **a** Individual mEPSCs resulting from a release of 1,500, 3,000 and 6,000 glutamate molecules with their best fits; **b, c** as the number of molecules released increases the amplitude rises, but not the decay time; **d, e** glutamate concentration in the cleft decreases multi-exponentially. The concentration is greater but less variable if more molecules are released; **g, h** the occupancy of the double bound (closed) state also rises and becomes less variable with more molecules released

of it. It is interesting to note that the decrease cannot be explained by the lower occupancy of the double bound state (which is in fact higher), but by its significantly lower variability (Fig. 10g, h). Both are associated with, and partly caused by the changes of the glutamate concentration in the cleft, which are similar (Fig. 10d, e). The occupancy of the desensitized state linked to the open state could play only a marginal role in modulating the median frequency. This

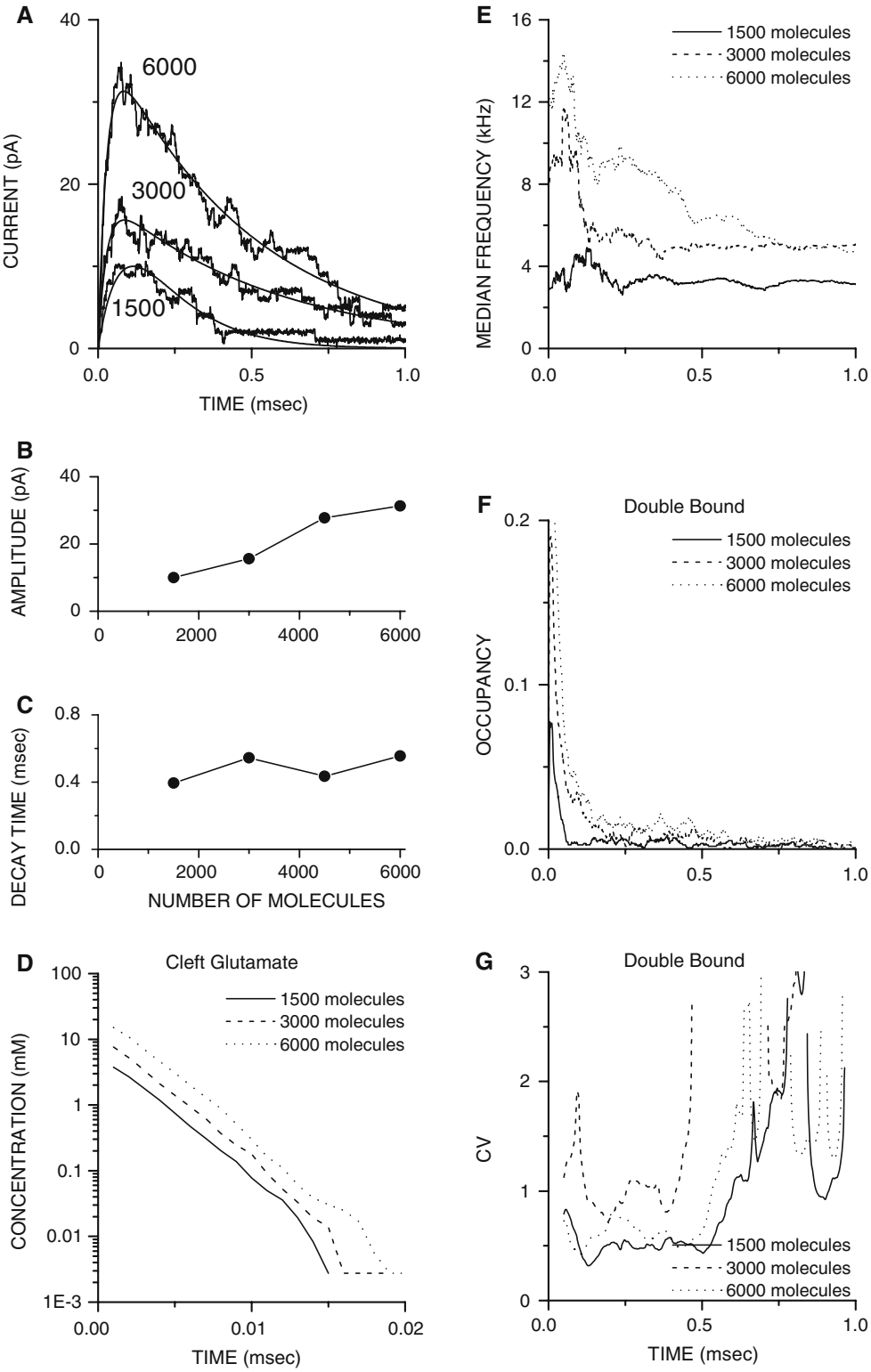

Fig. 9 Transient median frequency of the current fluctuations is much greater, when more glutamate molecules are released, if glutamate molecules are not able to return into the synaptic cleft (see text; **f**). **a** Individual mEPSCs resulting from a release of 1,500, 3,000 and 6,000 glutamate molecules with their best fits; **b, c** as the number of molecules released increases the amplitude rises, but not the decay time. Amplitudes are significantly smaller than those observed when molecules are able to return into the cleft (see Fig. 8); **d, e** glutamate concentration in the cleft decreases very rapidly and mono-exponentially reaching zero levels in 20–30 μs. **f, g** both the occupancy of the double bound (closed) state and its variability, are greater if more molecules are released

occupancy rises following the release of glutamate and the activation of AMPA receptors. Although it becomes greater than the occupancy of the double bound (closed) state, it is higher when the diffusion constant is lower. More importantly the occupancy of the desensitized state is always much too small to affect the current fluctuations, because the forward rate from this desensitized state into the open state is very low (see Sect. 2).

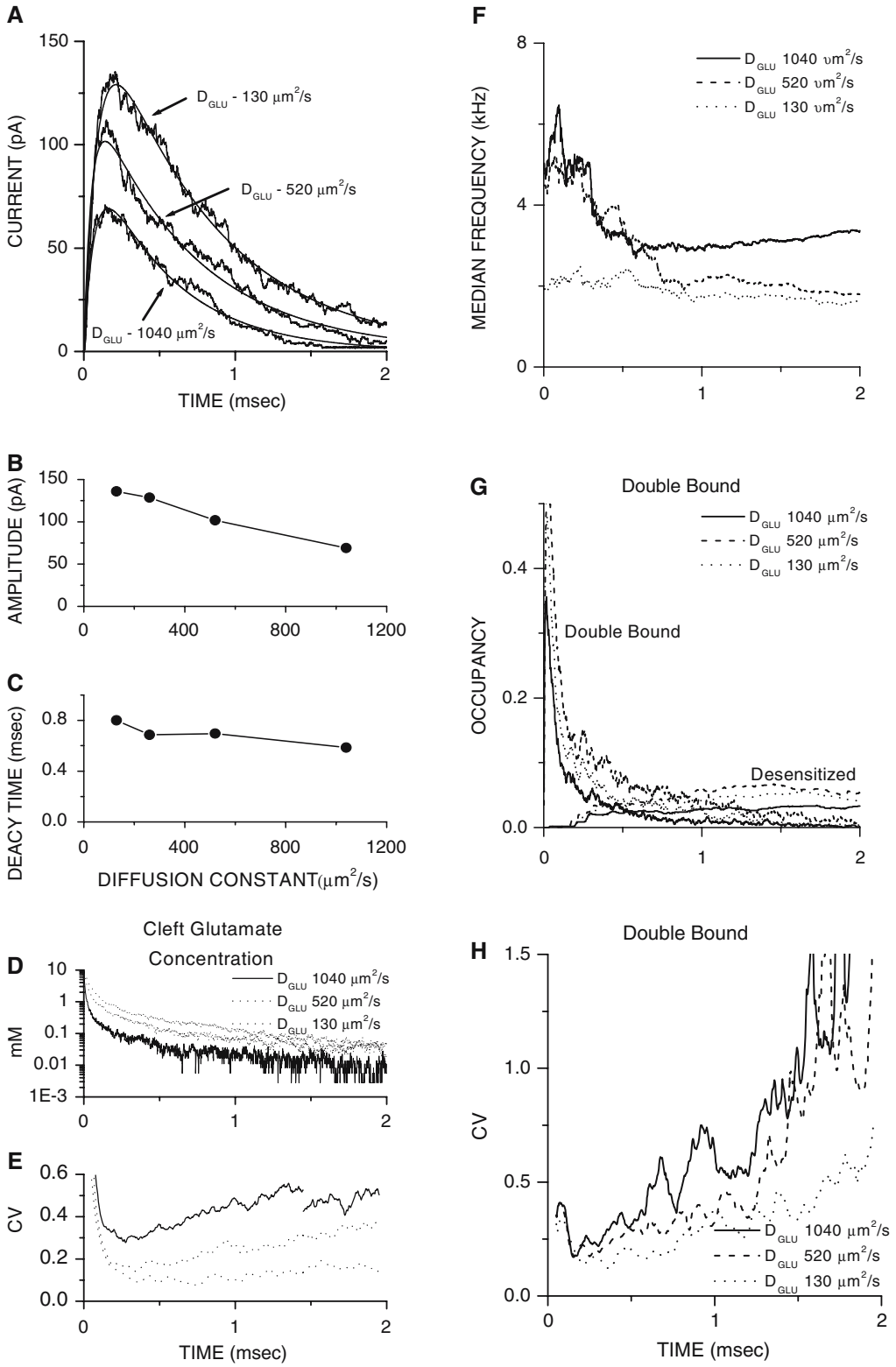

Fig. 10 The mEPSCs amplitude rises (**b**) whereas its decay time lengthens (**c**), when the diffusion constant decreases, but the transient median frequency diminishes greatly (**f**). **a** Individual mEPSCs resulting from a release of 3,000 glutamate molecules and with diffusion constant of glutamate being 1,040, 520 or 130 $\mu m^2 s^{-1}$ with their best fits; **d, e** glutamate concentration in the cleft rises, but becomes significantly less variable if diffusion constant decreases; **g, h** the occupancy of the double bound state (closed) also rises and becomes clearly less variable with slower diffusion. The occupancy of the desensitized state linked to the open state rises to the levels above those of the double bound (closed) state, but is unlikely to affect the current fluctuations (see text)

3.7 Lowering opening rate increases transient median frequency whereas lowering closing rate decreases steady-state median frequency

The amplitude of mEPSC also rises and its decay time lengthens even more clearly when the channel opening rate α increases (Fig. 11a, c). These changes are also associated with a smaller peak of the transient median frequency (Fig. 11f). Lower and less variable occupancy of the double bound state explain these changes (Fig. 11g, h). Note that the changes of the occupancy of the double bound state are not due to the changes of the cleft concentration since neither the glutamate concentration in the cleft nor its variability are affected (Fig. 11d, e). When the channel closing rate β decreases the mEPSC amplitude rises modestly, whereas its decay time lengthens very significantly (Fig. 12a–c). Although this is not associated with a significant change of the transient median frequency, the steady-state median frequency diminishes (Fig. 12f). The occupancy of the double bound state and its variability change but only modestly (Fig. 12g, h). Finally, as observed when the opening rates changed neither the glutamate concentration in the cleft nor its variability is affected (Fig. 12d, e).

3.8 Kalman-AR spectral estimation of the fluctuations of spontaneous excitatory post-synaptic currents in rat hippocampal pyramidal cells

Figure 13a gives a spontaneous excitatory post-synaptic current (mEPSC) recorded in rat hippocampal pyramidal cell together with the best fit by the sum of two exponentials calculated using the least squares fitting method. The best-fitted equation was: $i = 50.2 \times \exp^{-t/13.6} \times (1 - \exp^{-t/0.91})$. The recorded current fluctuations and their Kalman-AR-model prediction estimated using a second order AR-model are given in Fig. 13b, c respectively. The median frequency of the Kalman-AR prediction rises to a peak during the rise phase and early decay phase of the mEPSC, then decreases and finally settling to an apparent steady-state (Fig. 13d) in agreement with changes of median frequency observed for Monte-Carlo simulated current fluctuations. The variance estimate displayed a broader peak (Fig. 13e). Finally, the AR parameters estimated by the Kalman-AR-model fitting were smooth (Fig. 13f). The state noise variance σ_w^2 was 5×10^{-9}, the window for averaging the prediction error variance σ_ε^2 had 50 samples, and the initialization was 'static'. Its values were obtained from 100 samples segment at the start, which was passed through a static second order AR-model.

Figure 14 shows three spontaneous excitatory post-synaptic currents (mEPSCs) of different amplitudes recorded in the rat hippocampal pyramidal neuron (a_1, b_1 and c_1; three different cells), together with the best fits by the sum of two exponentials calculated using the least squares fitting method, and with the current fluctuations. The best-fitted equation was: $(a_1)i = 54.2 \times \exp^{-t/11.9} \times (1 - \exp^{-t/0.8})$, $(b_1)i = 21.4 \times \exp^{-t/9.1} \times (1 - \exp^{-t/0.85})$ and $(c_1)i = 25.1 \times \exp^{-t/10.1} \times (1 - \exp^{-t/0.73})$. The a_2, b_2 and c_2 depict the predicted fluctuations (Kalman-AR prediction), a_3, b_3 and c_3 give the changes of the corresponding median frequency of the Kalman-AR prediction of current fluctuations, which have their maxima during the rise phase or during early decay phase of the mEPSC. Their apparent steady-state median frequencies rise from ~0.5 kHz ($V_{hold} = -60$mV; a_3) to ~1.0 kHz ($V_{hold} = -80$mV; b_3) to ~1.4 kHz ($V_{hold} = -100$mV; c_3), a_4, b_4 and c_4 show the variance of the Kalman-AR prediction of the current fluctuations. The initial rise of the variance is followed by a decrease to the steady-state value, which is similar to the value at the start. The state noise variance σ_w^2 was 5×10^{-9}, the window for averaging the prediction error variance σ_ε^2 had 50 samples, and the initialization was 'static' (it used 100 samples from the segment at the start, and passed them through a static second order AR-model).

4 Discussion

4.1 Parametric spectral estimation of the non-stationary Monte-Carlo simulated excitatory post-synaptic current fluctuations—AR approach

The evaluation of power spectra using parametric methods differs significantly from the estimation using non-parametric methods such as Fourier and Wavelet analyses (Fishman 1973; Rioul and Vetterli 1991; Aristizabal and Glavinović 2003). The evaluation is not done directly from the data. Instead the data are modeled as the output of the linear time-invariant system, which is driven not by an unknown physiological input, but by white noise (Marmarelis and Marmarelis 1978). The parameters of such a linear system generating the observed signal are then estimated. Although this approach does not replicate the way the signals are generated, it is a highly effective method for estimation of their spectra. Another feature of the parametric model fitting—its ability to provide 'predicted time series' (i.e. the fluctuations 'predicted' by the model)—is especially useful, because a comparison with the actual time series (mEPSC current fluctuations) yields an insight into the ability of the model to fit the signal that is intuitively easy to grasp. Their additional strength is that they provide spectral estimations even when the precise nature of the modeled system is not known, and the kinetic scheme of ion channel gating is often unknown, or not known fully. The application of this method requires the signals (such as non-stationary excitatory post-synaptic current fluctuations) to be divided

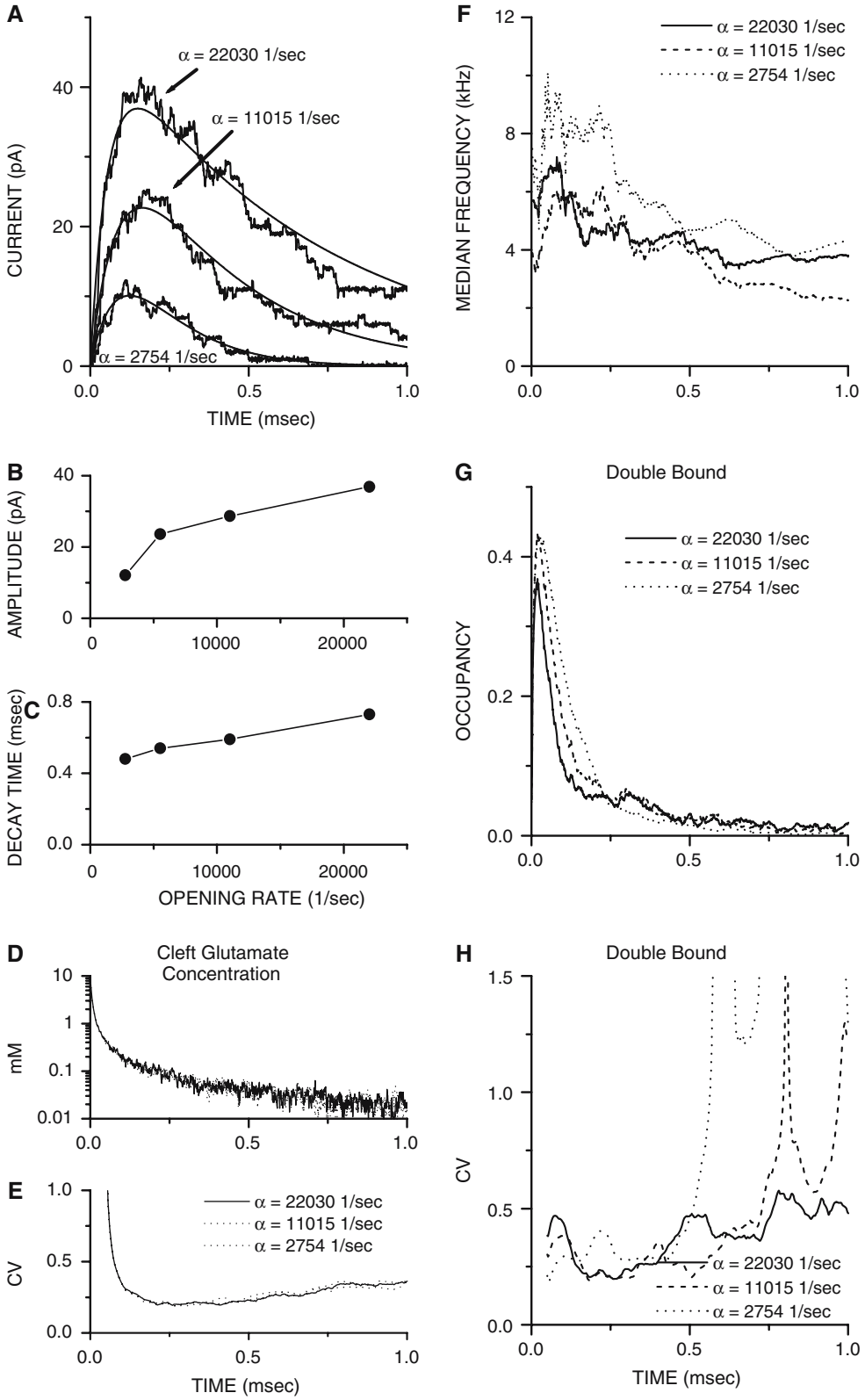

Fig. 11 The mEPSCs amplitude rises (**b**) and its decay time lengthens (**c**), when the channel opening rate α increases, but the transient median frequency tends to diminish (**f**). **a** Individual mEPSCs resulting from a release of 3,000 glutamate molecules and with the channel opening rate α being 22,030, 11,015 or 2,754 $1s^{-1}$, with their best fits; **d, e** neither the glutamate concentration in the cleft, nor its variability is affected by the changes of α; **g, h** the occupancy of the double bound state (closed) decreases, and becomes less variable as α rises. The median frequency and the occupancy of the double bound state are averages from six simulations

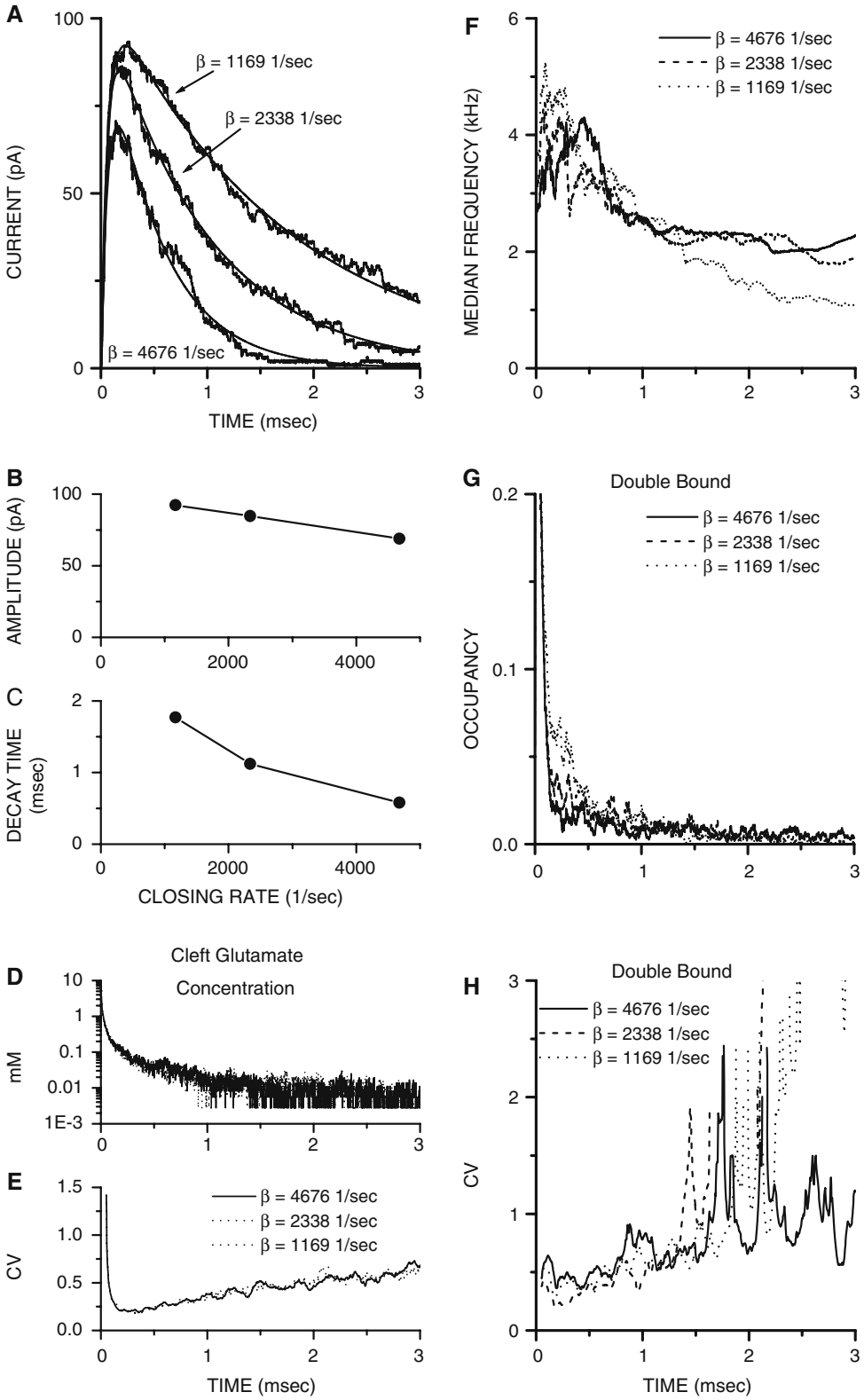

Fig. 12 The mEPSCs amplitude rises modestly (**a, b**) and the decay time lengthens significantly (**c**), when the channel closing rate β decreases, and these changes are associated with a lower steady-state median frequency (**f**). **a** Individual mEPSCs resulting from a release of 3,000 glutamate molecules and with the channel closing rate β being 1,169, 2,338 and 4,676 $1s^{-1}$, with their best fits; **d, e** neither the glutamate concentration in the cleft, nor its variability is affected by the changes of β; **g, h** the occupancy of the double bound state (closed) increases, and becomes more variable as β decreases, but not greatly

into short segments. An AR-model is subsequently fitted to each such segment, which is thus assumed to be piece-wise stationary and independent from other segments.

We used AR-models to fit the current fluctuations because the fitting algorithm is linear. Using more general ARMA models enables one to characterize more complex spectral

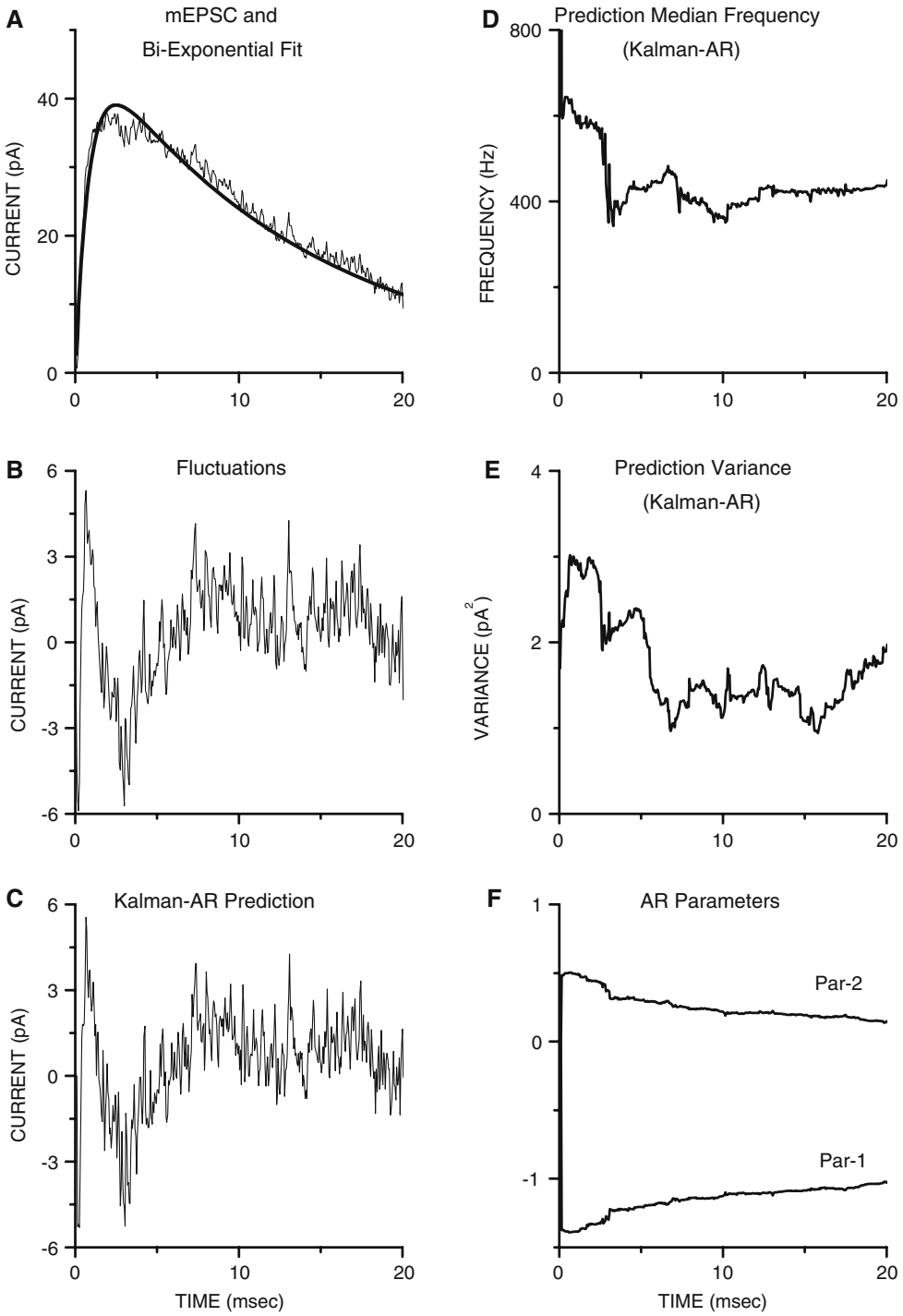

Fig. 13 Adaptive model fitting of the fluctuations of a spontaneous excitatory post-synaptic current (mEPSC) recorded in rat hippocampal pyramidal cell. **a** mEPSC with the best fit by the sum of two exponentials; **b** mEPSC fluctuations; **c** Kalman-AR-model prediction of the current fluctuations **d** The median frequency of the Kalman-AR prediction rises to a peak during the rise phase and early decay phase of the mEPSC, finally settling to an apparent steady-state; **e** the variance of the Kalman-AR prediction; **f** AR parameters estimated by the Kalman-AR-model fitting. Note that the time course of both parameters is smooth. The state noise variance σ_w^2 was 5×10^{-9} and the window for averaging the prediction error variance σ_ε^2 had 50 samples, and the initialization was 'static'. Holding potential was –60 mV, temperature was 27°C

shapes, but the spectra in these studies are simple, and are described by a single Lorentzian or a sum of several Lorentzians (i.e. the spectra are without peaks or notches). The model order, which determines how many of the previous data points are taken into account to calculate the chosen data point, also determines the complexity of the spectral shapes that can be fitted. Generally the order chosen should be greater than the expected number of peaks of the spectrum. If the order is too low the spectrum will be excessively smoothed, but if it is too high it will appear too noisy if spurious peaks are introduced. In practical terms the choice of model order was not difficult (the lowest order was typically chosen) since the spectra obtained were very comparable to each other for a wide range of model order values.

The performance of such AR-model fitting revealed however several shortcomings. Although the estimated spectra

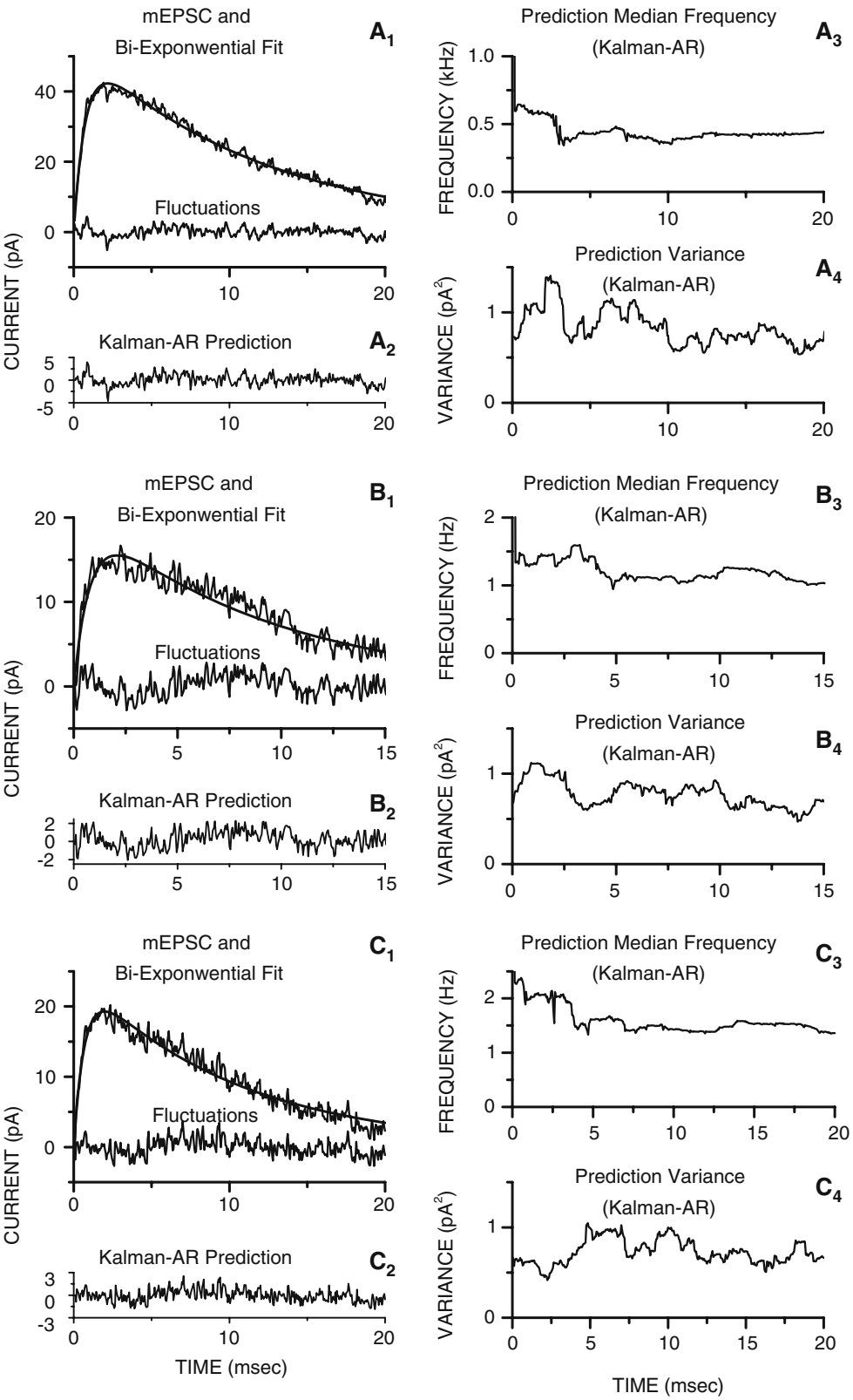

Fig. 14 Both the variance and the median frequency of the predicted fluctuations of spontaneous excitatory post-synaptic currents (mEPSCs; Kalman-AR prediction) recorded in rat hippocampal pyramidal neuron are higher during the rise or early decay phase of mEPSCs. The steady-state median frequency however, appears to depend on the holding membrane potential. $\mathbf{a}_1$, $\mathbf{b}_1$ and $\mathbf{c}_1$ mEPSCs, their bi-exponential fits and current fluctuations; $\mathbf{a}_2$, $\mathbf{b}_2$ and $\mathbf{c}_2$ Kalman-AR prediction of the current fluctuations; $\mathbf{a}_3$, $\mathbf{b}_3$ and $\mathbf{c}_3$ median frequency of the Kalman-AR prediction of current fluctuations. $\mathbf{a}_4$, $\mathbf{b}_4$ and $\mathbf{c}_4$ variance of the Kalman-AR prediction of the current fluctuations. The state noise variance σ_w^2 was 5×10^{-9} and the window for averaging the prediction error variance σ_ε^2 had 50 samples, whereas the initialization was 'static'. The holding potential was –60, –80 and –100 mV (**a**, **b** and **c**, respectively). The temperature was 20–22°C

were smooth and the predicted signal well reproduced the 'true' current fluctuations free of extraneous noise, the estimates of the median frequencies of current fluctuations and AR parameters were very scattered. The spectral smoothness of AR-model fits was due to inclusion of the noise term in the AR-model. As a result the estimates are based on the signal

from which most, if not all 'extraneous' noise was removed. This is in contrast to Fourier based spectral estimates, which are based on the contributions of both the signal (current fluctuations) and the 'extraneous' noise. The reasons for the scatter of the estimates of the median frequency are of a different nature, and are a consequence of an assumption that data in each window are independent from those in neighboring windows, and more importantly because the fluctuations are considered stationary within individual windows.

4.2 Generation of non-stationary signals by concatenation of stationary signals of different amplitude or by concatenation of time-varying AR parameters

The scatter of the estimates of the variance and of the median frequency of various signals can be much reduced with adaptive parametric model fitting. In adaptive models the values of the free parameters are updated with the arrival of each new data sample. The ability of such an adaptive parameter estimation method—Kalman-AR-model fitting—to accurately estimate the variance and the spectral properties of non-stationary synaptic current fluctuations had to be tested carefully. First, we generated two segments of stationary processes with different but constant variances and identical spectral properties, and concatenated them directly. The spectral evaluation of such concatenated signals is easy to understand, although they correspond to an unrealistic change of the physiological process, and at the points of discontinuity the spectral and variance estimates are problematic (i.e. where two processes of different spectral properties or variance are joined; Kaipio and Karjalainen 1997). Nevertheless, the Kalman-AR method accurately estimated and rapidly tracked the changes of variance of signal fluctuations. This is important, because the spectra of the synaptic current fluctuations are also simple and have a similar shape. They are described by a few, or even a single Lorentzian, and are also well characterized by low order AR-models.

Second, we tested the ability of Kalman-AR-model fitting to estimate AR parameters of signals whose spectral properties (and not only variance) change rapidly, and generated the non-stationary signals using second order AR-models with predefined time-varying parameters. AR-models have been used before to simulate non-stationary biological signals such as EEG signals (Kaipio and Karjalainen 1997; Isaksson et al. 1981; Arnold et al. 1998). Generating non-stationary fluctuations using AR-models enables one to directly verify the accuracy and tracking ability of the Kalman-AR method to estimate model parameters by directly comparing them with 'true' parameters (i.e. the parameters used for generation of non-stationary signals). Both parameters were generated by a concatenation of two sinusoids of identical amplitudes but different frequencies. Although this represents a concatenation of parametric representations of the segments without a discontinuity of the parameter values, it nevertheless defines a time-varying filter with the coefficients changing at the points of concatenation in a way unexpected from the changes occurring prior to the concatenation loci. Nevertheless Kalman-AR estimated AR parameters highly accurately even at the loci of concatenation. Taken together these tests argue that the Kalman-AR-model fitting should be able to estimate accurately and track rapidly the spectral changes of the current fluctuations that occur during the time course of mEPSCs.

4.3 Parametric spectral estimation of the non-stationary monte-carlo simulated excitatory post-synaptic current fluctuations – kalman-AR approach

The estimates of the median frequency were indeed less scattered with adaptive model fitting, irrespective of whether Kalman, RLS or LMS approaches were used. All three algorithms are recursive i.e. the estimate for each state is computed using updating equations. The tracking speed of all three methods is adjustable, but each method has a different tool for adjusting the speed of the algorithm. The state noise variance σ_w^2 controls the adaptation (i.e. it controls how much 'true' AR parameters are permitted to change; a random walk is assumed, with a white Gaussian noise) of Kalman-AR method. χ— forgetting factor and μ—the step size control the adaptation of RLS and LMS methods, respectively (Tarvainen et al. 2004). In all cases there is a trade-off between the tracking speed and the scatter of the parameter estimates, and faster tracking is associated with greater scatter of the estimated model parameters. Our choice of the value of the adaptation coefficient was based on the assessment of the quality of the signal prediction, but also on the visual inspection of the variables calculated from the model parameters. We however did not try to eliminate the lag between the current fluctuations and their Kalman-AR prediction, although the lag can be eliminated using the smoother algorithms (which utilize not only the past, but also the future measurements when calculating the parameters at a chosen time instant) together with Kalman filter (Tarvainen et al. 2004). In the present study the lag was small and was ignored.

The initialization of the Kalman-AR algorithm also affects the quality of the model fitting. Since it affects the quality of the estimates only during the convergence time of the algorithm, it is not critical when the signal is of adequate duration. In the present study, however, the signals were short and changed rapidly at the beginning, and this required a careful consideration. Using 'static' initialization reduced the convergence time for the estimation of AR parameters or variables (such as the median frequency of current fluctuations). How rapidly the filter is converging, when the signal is stationary, and how well it is adapting, when the signal is non-stationary, was also monitored using the mean learning rate.

The mean learning rate clearly decreased with time to low approximately steady-state levels.

4.4 Transient changes of frequency of current fluctuations depend on number of glutamate molecules released and their ability to return to synaptic cleft

The amplitude of mEPSC-s rises if more glutamate molecules are released, whereas the decay time remains unaltered. Amplitudes rise irrespective of whether molecules can re-enter into the cleft. However, the amplitudes are almost three times larger, if re-entrance from the peri-synaptic cleft (equally wide as the synaptic cleft and extending into the infinity) is allowed, whereas the decay times are longer but only marginally. Note however that in both cases the steady-state median frequency of current fluctuations is insensitive to how many molecules are released, or whether the molecular re-entry into the synaptic cleft occurs. By contrast the relationship of the transient median frequency of current fluctuations and the number of molecules released depends on the re-entry of glutamate molecules. If the molecular re-entry occurs the transient median frequency of current fluctuations diminishes though modestly as more molecules are released, whereas in the absence of the re-entry clearly increases.

In the absence of molecular re-entry into the synaptic cleft the transient median frequency rises when more molecules are released because the occupancy of the double bound state and its variability rise to higher levels. Cleft glutamate modulates the occupancy of the double bound state only initially, because the glutamate concentration diminishes to zero values in 20–30 μs and has no effect subsequently. However, if re-entry occurs and is significant the cleft glutamate will persist during the rise phase and decay phase of an mEPSC altering the occupancy of the double bound state and the current fluctuations. If more molecules are released the cleft glutamate concentration rises but modestly, whereas its variability in the cleft diminishes significantly. Their net effect is lower median frequency of the current fluctuations.

4.5 Transient changes of frequency of current fluctuations depend on diffusion constant of glutamate in synaptic cleft

Diffusion constant of glutamate in the synaptic cleft is unknown. It is typically assumed to be the same as in the physiological bulk solution (Wahl et al. 1996; Glavinović 2002; Ventriglia 2004), but significantly lower values have also been assumed (Kleinle et al. 1996) and a recent study suggests that the diffusion constant may be ∼1/3 of the value for free diffusion in water (Nielsen et al. 2004). However, recent molecular dynamics simulations of diffusion of glutamate in the confined space of the synaptic cleft have shown that the diffusion constant is reduced only if the cleft is very narrow. If the cleft width is as morphometric studies in the central nervous system have shown the glutamate$^-$ diffusion should not be slowed by the confinement or membrane charges and thus is likely to be similar to that in the free solution (Cory and Glavinović 2006). Nevertheless, we consider it prudent to evaluate how slower diffusion would affect the amplitude and the time course of mEPSCs and their current fluctuations. The amplitude of mEPSCs rises if the diffusion constant of glutamate in the synaptic cleft decreases. Since the decay time increases only modestly these changes are similar to those seen when the number of glutamate molecules released rises and the molecular re-entry is allowed. However, the peak of the transient median frequency of current fluctuations decreases much more. Although the underlying causes of lower transient median frequency are the same, the balance is different because the cleft glutamate concentration, and the overall occupancy of the double bound state are only moderately higher, whereas the variability of the concentration, and the occupancy of the double bound state are much lower.

4.6 Closing rate alters steady-state frequency and opening rate transient frequency of current fluctuations

Greater opening rate α, and to a lesser extent lower closing rate β also enhance the amplitude of mEPSCs. However, these changes, but especially lower β significantly lengthen the decay time of mEPSCs. Their effects on the median frequency however, are very different. The transient median frequency of current fluctuations diminishes if α rises, whereas the steady-state median frequency diminishes when β decreases. These changes of median frequency are not due to the changes of the cleft glutamate concentration modulating the occupancy of the double bound state or its variability, because neither the overall cleft concentration nor its variability changed significantly.

4.7 Kalman-AR-model fitting of the non-stationary excitatory post-synaptic current fluctuations in rat hippocampal pyramidal neurons

The spectral changes during the time course of individual quantal events in pyramidal neurons of rat hippocampus are also rapid, but they can similarly be estimated accurately and tracked rapidly using Kalman-AR-model fitting of individual mEPSCs. This is important because the channel properties underlying individual quantal events in the central nervous system may differ from one bouton to another. The median frequency of the current fluctuations typically has a maximum near the peak of the mEPSC. Subsequently, the median

frequency reaches an apparent steady state, as observed for Monte-Carlo simulated current fluctuations. The steady-state median frequency rises when the holding potential becomes more hyperpolarized revealing a voltage dependence of the closing rate of AMPA channels. The estimates of the peak median frequency of the current fluctuations of recorded mEPSCs were typically less elevated than those of simulated mEPSCs. This is also not surprising given that in all simulations the release occurred from an instantaneous point source, whereas physiologically the release occurs from the vesicle and through the fusion pore, and is not instantaneous. Alternative explanation is that the diffusion constant of glutamate in the synaptic cleft is lower than in the bulk. The time course of variance of current fluctuations is also available from the Kalman-AR-model fits to individual quantal events. They are thus uncontaminated by the variable contribution of 'instantaneous' glutamate concentration (Kruk et al. 1997; Glavinović 1999), although the rapidly developing desensitization of AMPA receptors limits their usefulness in determining the number of AMPA receptors post-synaptically using a binomial theorem (Aristizabal and Glavinović 2003). Nevertheless the changes of variance and median frequency of current fluctuations are likely to provide useful information about the gating kinetics of AMPA channels and the time course of glutamate in the synaptic cleft. Full examination of these questions is however beyond the scope of this paper.

5 Conclusion

This study demonstrates the ability of time-variant Kalman-AR-models to accurately fit the fluctuations of Monte-Carlo simulated excitatory post-synaptic currents or currents recorded from pyramidal neurons of rat hippocampus. The median frequency of current fluctuations could be rapidly tracked and estimated from the individual quantal events. It showed an early transient peak before declining to a steady-state level. The steady-state median frequency is largely determined by the closing rate of AMPA receptors, but the transient peak can be modulated by a variety of factors—number of molecules released, ability of glutamate molecules to re-enter the synaptic cleft, diffusion constant of glutamate in the cleft and opening rate. In each case the effect on the amplitude and decay time of mEPSCs and on the current fluctuations is quite different. Each thus appears to leave its own kinetic fingerprint arguing that these factors can be inferred from the kinetic properties of individual mEPSCs.

Acknowledgements This work was supported by the grant from the National Sciences and Engineering Research Council of Canada to M.I.G. Dr. K. Krnjevic read the manuscript and made valuable comments

References

Aristizabal F, Glavinović MI (2003) Wavelet analysis of Monte-Carlo simulated excitatory pots-synaptic currents. Biophys J 85:2170–2185

Arnold M, Miltner H, Witte H, Bauer R, Braun C (1998) Adaptive AR-modeling of nonstationary time series by means of Kalman filtering. IEEE Trans Biomed Eng 45:553–562

Benke TA, Luthi A, Palmer MJ, Wikstrom MA, Anderson WW, Isaac JTR, Collingridge GL (2001) Mathematical modeling of non-stationary fluctuation analysis for studying channel properties of synaptic AMPA receptors. J Physiol 537:407–420

Clements JD (1996) Transmitter time course in the synaptic cleft: its role in central synaptic function. Trends Neurosci 19:163–171

Colquhoun D, Jonas P, Sakmann B (1992) Action of brief pulses of glutamate on AMPA/kainate receptors in patches from different neurones of rat hippocampal slices. J Physiol Lond 458:261–287

Cory SM, Glavinović MI (2006) Molecular dynamics simulations of glutamate diffusion in synaptic cleft. Crit Rev Neurobiol 18:47–55

DeFreitas JFG, Niranjan M, Gee AH (1998) Hierarchical Bayesian-Kalman models for regularisation and ARD in sequential learning. Tech Report CUED/F-INFENG/TR 307, Dept Eng, Cambridge Univ, UK

Derksen HE, Verveen A (1966) Fluctuations of resting neural membrane potential. Science 151:1388–1389

Dingledine R (ed) (1984) Brain slices. Plenum, New York

Fishman HM (1973) Relaxation spectra of potassium channel noise from squid axon membranes. Proc Natl Acad Sci USA 70:876–879

Franks KM, Stevens CF, Sejnowski TJ (2003) Independent sources of quantal variability at single glutamatergic synapses. J Neurosci. 23:3186–3195

Glavinović MI, Rabie H (1998) Monte-Carlo simulation of spontaneous miniature excitatory postsynaptic currents in rat hippocampal synapse in the presence and in the absence of desensitization. Pflugers Arch 435:193–202

Glavinović MI (1999) Monte-Carlo simulation of vesicular release, spatio-temporal distribution of glutamate in synaptic cleft, and generation of postsynaptic currents. Pflugers Arch 437:462–470

Glavinović MI (2002) Mechanisms shaping fast excitatory postsynaptic currents in the central nervous system. Neural Comp 14:1–19

Grenier Y (1983) Time-dependent ARMA modeling of non-stationary signals. IEEE Trans Acoust Speech Signal Process 31:899–911

Haykin S (1986) Adaptive filter theory. Prentice Hall, Englewood Cliffs

Hirasawa H, Shiells R, Yamada M (2001) Blocking AMPA receptor desensitization prolongs spontaneous EPSC decay times and depolarizes H1 horizontal cells in carp retinal slices. Neurosci Res 40:217–225

Isaacson JS, Nicoll RA (1991) Aniracetam reduces glutamate receptor desensitization and lows the decay of fast excitatory synaptic currents in the hippocampus. Proc Natl Acad Sci USA 88:10936–10940

Isaksson A, Wennberg A, Zetterberg L (1981) Computer analysis of EEG signals with parametric models. Proc IEEE 69:451–461

Jackson MF, Joo DT, Al-Mahrouki AA, Orser BA, Macdonald JF (2003) Desensitization of alpha-amino-3-hydroxy-5-methyl-4-isoxazolepropionic acid (AMPA) receptors facilitates use-dependent inhibition by pentobarbital. Mol Pharmacol 64:395–406

Jonas P, Major G, Sakmann B (1993) Quantal components of unitary EPSCs at the mossy fibre synapse on CA3 pyramidal cells of rat hippocampus. J Physiol Lond 472:615–663

Jones MV, Westbrook GL (1996) The impact of receptor desensitization on fast synaptic transmission. Trends Neurosci 19:96–101

Kaipio J, Karjalainen P (1997) Simulation of nonstationary EEG. Biol Cybern 76:349–356
Kalman R (1960) A new approach to linear filtering and prediction problems. Trans ASME J Basic Eng 82:35–45
Katz B, Thesleff S (1957) A study of the desensitization produced by acetylcholine at the motor end-plate. J Physiol Lond 138:63–80
Katz B, Miledi R (1972) The statistical nature of the acetycholine potential and its molecular components. J Physiol Lond 224:665–699
Kleinle J, Vogt K, Luscher HR, Muller L, Senn W, Wyler K, Streit J (1996) Transmitter concentration profiles in the synaptic cleft: an analytical model of release and diffusion. Biophys J 71:2413–2426
Krnjević K, Glavinović MI (1999) Use of parametric analysis to evaluate number and kinetics of post-synaptic receptors. Soc Neurosci Abstr 25:992
Kruk PJ, Korn H, Faber DS (1997) The effects of geometrical parameters on synaptic transmission: a Monte-Carlo simulation study. Biophys J 73:2874–2890
Longsworth LG (1953) Diffusion measurements at 25°C, of aqueous solutions of amino acids, peptides and sugars. J Amer Chem Soc 75:5705–5709
Marmarelis PZ, Marmarelis VZ (1978) Analysis of physiological systems. Plenum, New York
Mozrzymas JW (2004) Dynamism of GABA(A) receptor activation shapes the "personality" of inhibitory synapses. Neuropharmacology 47:945–960
Nielsen TA, DiGregorio DA, Silver RA (2004) Modulation of glutamate mobility reveals the mechanism underlying slow-rising AMPAR EPSCs and the diffusion coefficient in the synaptic cleft. Neuron 42:757–771
Pardey J, Roberts S, Tarassenko L (1996) A review of parametric modeling techniques for EEG analysis. Med Eng Phys 18:2–11
Penny WD, Roberts SJ (1999) Dynamic models for nonstationary signal segmentation. Comp Biomed Res 32:483–502
Rao TS (1970) The fitting of non-stationary time series models with time dependent parameters. J R Stat Soc B 32:312–322
Rioul O, Vetterli M (1991) Wavelets and signal processing. IEEE Sig Proc 8:14–38
Robinson HPC, Sahara Y, Kawai N (1991) Nonstationary fluctuation analysis and direct resolution of single channel currents at postsynaptic sites. Biophys J 59:295–304
Sakmann B, Patlak J, Neher E (1980) Single acetylcholine-activated channels show burst-kinetics in presence of desensitizing concentrations of agonist. Nature 286:71–73
Sayed A, Kailath T (1994) State-space approach to adaptive RLS filtering. IEEE Signal Process Mag 11:18–60
Schlogl A (2000) The electroencephalogram and the adaptive autoregressive model: theory and applications. PhD dissertation, Dept. Med. Informatics, Inst Biomed Eng Univ Technol Graz, Austria
Silberberg SD, Magleby KL (1993) Preventing errors when estimating single channel properties from the analysis of current fluctuations. Biophys J 65:1570–1584
Tarvainen MP, Hiltunen JK, Ranta-aho PO, Karjalainen PA (2004) Estimation of nonstationary EEG with kalman smoother approach: an application to event-related synchronization (ERS). IEEE Trans Biomed Eng 51:516–524
Traynelis SF, Jaramillo F (1998) Getting the most out of noise in the central nervous system. Trends Neurosci 21:137–145
Trussell LO, Fischbach GD (1989) Glutamate receptor desensitization and its role in synaptic transmission. Neuron 3:209–218
Ventriglia F (2004) Saturation in excitatory synapses of hippocampus investigated by computer simulations. Biol Cybern 90:349–59
Wahl LM, Pouzat C, Stratford KJ (1996) Monte-Carlo simulation of fast excitatory synaptic transmission at a hippocampal synapse. J Neurophysiol 75:597–608
Wall MJ, Robert A, Howe JR, Usowicz MM (2002) The speeding of EPSC kinetics during maturation of a central synapse. Eur J Neurosci 15:785–797
Welch G, Bishop G (2002) An introduction to the Kalman filter. Tech. Report TR 95-041. Dept Comp Sci, Univ North Carolina at Chapel Hill. http://www.cs.unc.edu/~welch
Yelshansky MV, Sobolevsky AI, Jatzke C, Wollmuth LP (2004) Block of AMPA receptor desensitization by a point mutation outside the ligand-binding domain. J Neurosci 24:4728–4736